J. Fluid Mech. (1991), *vol.* 228, *pp.* 513–547
Printed in Great Britain

Effects of rotation on convective turbulence

By HARINDRA J. S. FERNANDO[1], RUI-RONG CHEN[2]† AND DON L. BOYER[2]‡

[1] Mechanical and Aerospace Engineering, Arizona State University, Tempe, AZ 85287-6106, USA

[2] Mechanical Engineering, University of Wyoming, Laramie, WY 82071, USA

(Received 19 May 1989 and in revised form 7 January 1991)

Laboratory experiments were carried out to investigate the effects of rotation on turbulent convection. The experimental facility was a bottom-heated, water-filled, cubical tank mounted on a turntable. The investigations were performed over a wide range of bottom buoyancy fluxes q_0 and rotation rates Ω, including $\Omega = 0$; q_0 and Ω were held constant during each experiment. The depth of the water column H was fixed for the entire experimental programme. For the non-rotating experiments, the r.m.s. velocity fluctuations were found to scale well with the convective velocity $w_* = (q_0 H)^{\frac{1}{3}}$, while the mean and r.m.s. fluctuations of buoyancy were found to scale with q_0/w_*. The spectra of temperature fluctuations were measured and were used to assess the applicability of two types of scaling, one of which is advanced in the present study.

For the rotating experiments, the convective-layer growth is affected by the rotation at a height $h_c \approx 4.5(q_0 \Omega^{-3})^{\frac{1}{2}}$. The r.m.s. horizontal velocity of the rotationally affected mixed layer is uniform throughout the mixed layer and is given by $(\overline{u'^2})^{\frac{1}{2}} \approx 1.7(q_0 \Omega^{-1})^{\frac{1}{2}}$. The time growth law of the mixed-layer thickness h_r, when $h_r > h_c$, is given by $h_r \approx 0.7(q_0 \Omega^{-3})^{\frac{1}{2}} \Omega t$, where t is the time. The rotational effects become important when the Rossby number is given by $Ro = (\overline{u'^2})^{\frac{1}{2}}/\Omega l_r \approx 1.5$, where the integral lengthscale is estimated as $l_r \approx 0.25 h_c$. The mean buoyancy gradient in the mixed layer was found to be much higher than in the corresponding non-rotating case, and the r.m.s. fluctuations and mean buoyancies were found to scale satisfactorily with $(q_0 \Omega)^{\frac{1}{2}}$. A spectral form for the temperature fluctuations in rotating convection is also proposed and is compared to the experimental results.

1. Introduction

Turbulent thermal convection occurs in many engineering and geophysical flow situations. These include, for example, metal solidification processes, heat exchanger systems, the atmospheric daytime boundary layer, the upper-oceanic winter mixed layer and the solid core of the Earth. One of the simplest cases of turbulent thermal convection is that in which a wide, horizontal, homogeneous, fluid layer is heated from below and/or cooled from above. Properties of such flow configurations, for example transition to turbulence and the intensity and energetics of the turbulence itself, have been studied extensively; see for example, the review by Adrian, Ferreira & Boberg (1986). When additional factors such as stratification, double diffusion,

† Visiting Scientist from Institute of Atmospheric Physics, Academia Sinica, Beijing, China.

‡ Present address: Mechanical and Aerospace Engineering, Arizona State University, Tempe, AZ 85287-6106, USA.

magneto-hydrodynamic forcing, rotation or some combination thereof are included, the complexity of the convection process increases considerably. Because of the importance of stratification in the dynamics of atmospheric and oceanic mixed layers, this effect has been studied in some detail both experimentally and theoretically: recent reviews have been made by Deardorff (1985), Turner (1986) and Fernando, Boyer & Chen (1989). With the realization that double-diffusive convection can be an important mixing mechanism in the ocean, especially in the polar regions, numerous recent investigations have addressed this phenomenon. Huppert & Turner (1981), Chen & Johnson (1984) and Turner (1985) have discussed a variety of application areas in which double-diffusive convection plays an important role and have also carefully reviewed the range of recent research in this area.

In spite of its apparent relevance to atmospheric and oceanic mixed-layer turbulence, very little attention has been given to thermal convection in the presence of background rotation. Only a few laboratory studies have been reported in this context and almost all of them deal with either the transitional characteristics (Nakagawa & Frenzen 1955; Rossby 1969) or the initial development of the turbulent convection (Dikarev 1983; Boubnov & Golitsyn 1986). There have been a number of laboratory experiments (e.g. Traugott 1958; Ibbetson & Tritton 1975; Wigeland & Nagib 1978; Colin de Verdiere 1980; Hopfinger, Browand & Gagne 1982; Dickinson & Long 1983; Mory & Hopfinger 1988; Jacquin, Leuchter & Geoffroy 1989) and direct numerical simulations (e.g. Bardina, Ferziger & Rogallo 1985; Dang & Roy 1985) on the effects of rotation on shear-free, mechanically induced, homogeneous turbulence.

One of the possible reasons for the paucity of effort in the area of convection in rotating fluids may be the widespread belief among atmospheric scientists that the Earth's Coriolis forces are not important in determining the turbulence structure of the planetary boundary layer (PBL). The earlier notion that the PBL height should be scaled with u_*/f (Monin 1970; Tennekes 1970), where u_* is the surface friction velocity and f is the planetary vorticity, has been refuted on the basis of the large-eddy simulation studies of Deardorff (1970*a*, *b*; 1972); Deardorff's investigations have indicated clearly that the most appropriate length- and velocity scales for the PBL are the height of the mixed layer h and the convective velocity scale w_*, respectively. Here w_* is defined as

$$w_* = (q_0 h)^{\frac{1}{3}}, \tag{1}$$

where $q_0 = \alpha g Q/\rho_0 c_p$ is the buoyancy flux due to the bottom (surface) heat flux Q, α the coefficient of thermal expansion, g the gravitational acceleration, ρ_0 a reference density and c_p the specific heat at constant pressure. This result is physically plausible on the basis of Lilly's (1968) argument that surface friction is unimportant at heights z greater than the absolute value of the Monin–Obukhov lengthscale $|L|$; for the unstable atmosphere $h \approx 1$–2 km and $|L| \approx 100$ m.

The two cases, convection with and without rotation, are widely different; the former is essentially determined by the (flux) Rayleigh number Ra_f whereas in the latter, an additional variable, the Taylor number Ta, becomes important. For the case of convection driven by a constant bottom heat flux, these numbers are defined as $Ra_f = g_0 H^4/k_T^2 \nu$ and $Ta = 4\Omega^2 H^4/\nu^2$ where H is the depth of the fluid layer, k_T the thermal diffusivity, ν the kinematic viscosity and Ω is the rate of rotation (in rad s^{-1}). A study covering a range of Ra_f and Ta has recently been conducted by scientists of the USSR Academy of Sciences; this work has been published in Boubnov & Golitsyn

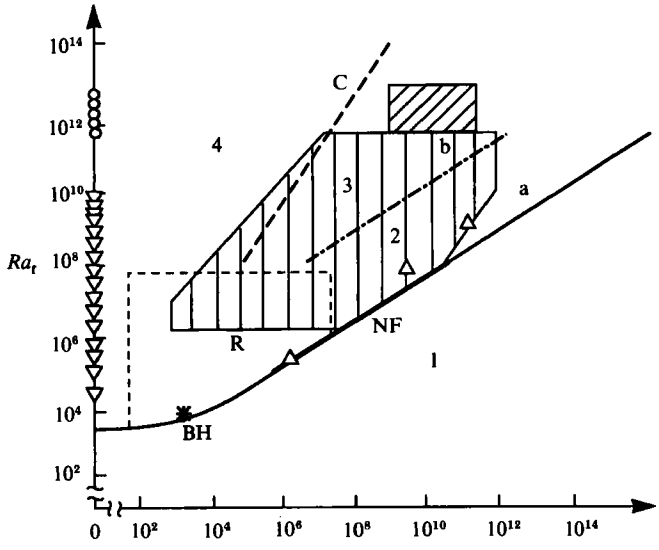

FIGURE 1. (Ra_f, Ta)-plane depicting the parameter ranges studied by various investigators (Courtesy of Dr B. Boubnov). For a description of the symbols, see the text.

(1986, 1988, 1990) and Boubnov & Ivanov (1988). The Ta and Ra_f ranges used in their studies are shown in figure 1 (vertical hatched lines). The experiments corresponding to the $\Omega = 0$ case are depicted along the Ra_f axis by inverted triangle symbols. Also included are the experiments of Rossby (1969) (Region R), Nakagawa & Frenzen (1955) (solid line NF) and Busse & Heikes (1980) [* symbol]. The parameter ranges of the experiments to be described in this paper are indicated by the diagonally hatched region and by the open circle symbols along the Ra_f axis. Boubnov & Golitsyn have subdivided the (Ra_f, Ta)-plane into different regimes, as shown in figure 1, viz.,

Region 1:	Conduction regime
(boundary a):	Chandrasekhar boundary (linear stability theory)
Region 2:	Regular structure
Region 3:	Geostropic turbulence
Region 4:	Fully developed turbulence

Note that the parameter ranges considered in the present study complement those of previous investigations.

The present research is an experimental study of the growth of a convective mixed layer in a homogeneous, rotating fluid with an emphasis on determining the structure of the resulting turbulence. The study was motivated by a number of factors. Although Deardorff's (1970*a*, *b*, 1972) large-eddy simulation results are generally accepted as being correct, they have not been subjected to experimental verification. The field data are usually contaminated by more than one physical process and cannot be unambiguously used to test such models. Even if u_* is unimportant and u_*/f is the incorrect scaling length above the surface layer ($z > |L|$), one cannot conclude that the Coriolis forces are unimportant because of the possibility that w_*/f can act as the relevant lengthscale. This lengthscale has not attracted as much attention as u_*/f in the PBL literature and it will be important to investigate its

significance. The dynamo processes responsible for the maintenance of planetary magnetic fields are governed by convective motions in the liquid nuclei of planets, and thus the studies on rotating convection are of direct interest to geo- and planetary physical studies. Further, the problem of the interaction between convective turbulence and rotation is of fundamental importance and deserves study for its inherent scientific interest.

2. Experimental procedure

The experimental facility is a cubical Plexiglas (1.25 cm thick) tank of dimensions $60 \times 60 \times 60$ cm and is shown in figure 2. This is the same facility used by Fernando *et al.* (1989) to study convective mixed-layer growth in non-rotating fluids. The tank bottom consists of a 1 cm thick aluminium plate; heating pads were placed below this plate. The heating system was insulated by placing two layers of 1.25 cm marsonite sheets, a single layer of 2.5 cm foam insulation and a 0.8 cm thick aluminium base plate beneath the heating pads. The maximum achievable heat (buoyancy) flux to the tank was 10 kW m^{-2} (10^{-5} m^2 s^{-3}). The sides of the tank were insulated using 1.25 cm thick styrofoam boards; one of the boards was removable to facilitate flow visualization and particle-streak photography. The test facility was positioned on a turntable capable of providing rotation rates Ω in the range $0.1 \leqslant \Omega \leqslant 1.0$ rad s^{-1}. The heat flux Q could be varied using a potentiometer. For a given experiment, however, a constant heat flux was used. The potentiometer was calibrated by measuring the temperture rise of a known mass of water contained in the tank for a given potentiometer setting; see Fernando (1987*a*). In evaluating the bulk experimental parameters such as the flux Rayleigh number Ra_f and Taylor number Ta, the physical properties of the fluid at the mean experimental temperature T_e were used; they are given in table 1.

Initially, the tank was filled to a 50 cm height either with pure water or with a homogeneous salt solution. The depth of the water column was always held constant to maintain a constant aspect ratio, so as to eliminate possible unwanted effects due to aspect-ratio changes. Temperature measurements were made using thermistor probes. To prevent deterioration of the probes these experiments were conducted solely in distilled water. Experiments in which velocity measurements were made were carried out separately; these utilized a homogeneous salt water solution having a specific gravity of 1.04, so that the polystyrene tractor particles used were approximately neutrally buoyant.

Some of the problems associated with this particular flow configuration are the restriction of horizontal motions by the sidewalls of the tank, possible formation of quasi-steady circulation patterns due to the difference in temperature gradients at the centre of the tank and at the walls, and the somewhat ill-defined boundary conditions at the top water level. Studies on thermal convection in homogeneous non-rotating fluids reveal that the integral lengthscale of convective eddies is approximately given by $l \approx 0.25H$. For the present case, $l \approx 12.5$ cm $\ll 60$ cm and it is possible to assume that the sidewalls will have an insignificant effect on r.m.s. turbulent quantities. The scale of possible large-scale secondary circulations, however, is of the same size as H; such motions are expected to be affected by the sidewalls. Nonetheless, the experiments of Townsend (1959), which have been carried out using a convection chamber of dimensions $30 \times 40 \times 56$ cm, indicate that the turbulent transport by these large-scale motions is insignificant, a fact which is corroborated by the work of Hopfinger & Toly (1976); the latter workers find that

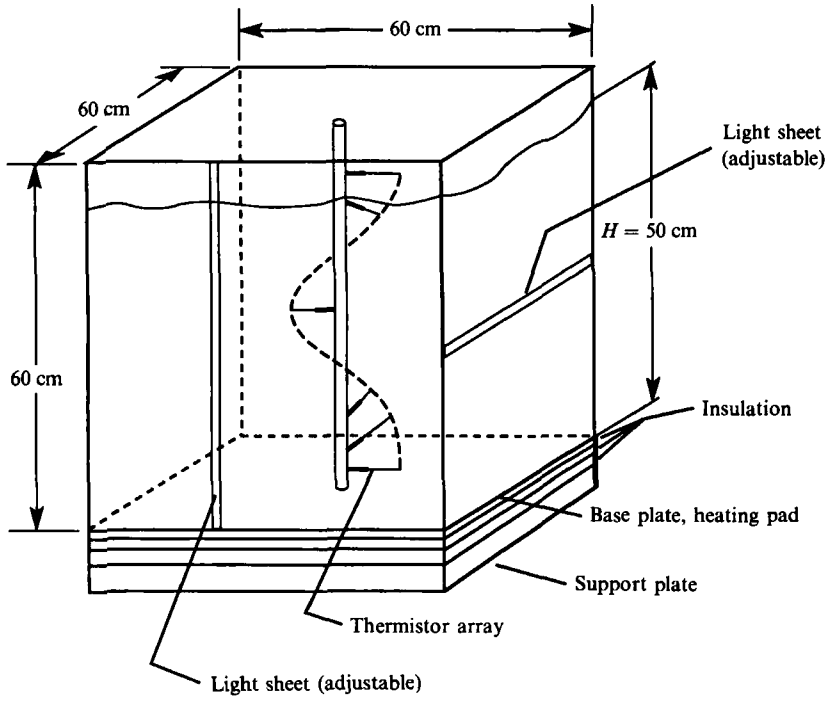

FIGURE 2. Schematic of test cell.

the energy of the large-scale secondary motions trapped between the sidewalls in mixing-box experiments is less than about 10% of the total turbulent kinetic energy. Analysis of data obtained from laboratory convection experiments with free surfaces (Willis & Deardorff 1974), during atmospheric free convection with an inversion at the top of the convective layer (Kaimal *et al.* 1976), from parallel plate experiments (Adrian *et al.* 1986) and using numerical simulations (Zeman & Lumley 1976) show that the nature of the top boundary does not significantly affect the nature of the convective turbulence (Adrian *et al.* 1986). As pointed out by Hunt (1984), the influence of the boundaries disappears after about one integral lengthscale away from them. Accordingly, it is reasonable to expect that convection experiments performed with different boundary conditions have some common features with regard to the properties of turbulence.

The thermal boundary condition at the free surface must be considered carefully. Because the free-surface temperature rise during an experiment is 0.3–2.4 °C and because the experiments last only a short period of time, the surface heat loss to the environment is typically less than 0.01% of the input power. Hence, in the analysis, the free surface is considered as an approximately thermally insulated boundary.

Both non-rotating and rotating experiments were conducted. In the latter case, the rotation rate was fixed at the desired level and approximately one hour was allowed for the working fluid to reach solid-body rotation prior to initiating the heating. The heaters were set at the desired Q and the heating was initiated at time $t = 0$.

During the early stages of an experimental run, a conduction layer developed along the bottom of the tank. This layer then broke down to form an upward-propagating turbulent mixed layer. The Rayleigh flux number Ra_f was of the order of 10^{12}–10^{13} and hence the convection in the tank could be considered as fully turbulent.

Run no.	Ω (rad s^{-1})	$q_0 \times 10^6$ (m^2 s^{-3})	T_e (°C)	$\nu \times 10^6$ (m^2 s^{-1})	$k_T \times 10^7$ (m^2 s^{-1})	$Ra_t \times 10^{-12}$	$Ta \times 10^{-10}$
		(*a*) Experiments with temperature measurements					
4	0	1.44	25.7	0.995	1.441	4.30	0
6	0	0.75	22.8	1.015	1.429	2.26	0
8	0	0.39	23.2	1.011	1.134	1.17	0
10	0	2.25	27.5	0.991	1.448	6.80	0
12	0.25	2.25	24.5	1.001	1.436	6.80	1.55
14	0.25	0.75	24.1	1.004	1.435	2.26	1.54
16	0.25	1.51	24.0	1.004	1.434	4.56	1.54
18	0.25	3.00	24.8	0.999	1.438	9.06	1.56
5	0.50	1.44	28.1	0.991	1.452	4.30	6.35
9	0.50	0.75	24.7	1.000	1.437	2.26	6.24
11	0.50	2.25	25.2	0.997	1.439	6.80	6.27
26	0.50	3.00	25.9	0.994	1.442	9.05	6.31
13	0.75	2.25	25.4	0.996	1.440	6.80	14.1
20	0.75	0.75	24.0	1.004	1.434	2.26	13.9
21	0.75	1.51	25.3	0.996	1.44	4.56	14.1
24	0.75	3.00	25.7	0.995	1.441	9.06	14.1
17	1.0	2.25	25.9	0.994	1.442	6.79	25.2
19	1.0	1.51	25.8	1.006	1.434	4.55	24.6
22	1.0	3.00	25.8	0.995	1.442	9.06	25.2
15	1.0	0.75	24.4	1.002	1.436	2.26	24.8
		(*b*) Experiments with velocity measurements					
33	0	1.51	25.7	0.995	1.441	4.56	0
60	0	1.30	25.5	0.996	1.440	3.92	0
64	0	2.07	27.2	0.991	1.448	6.22	0
66	0	0.61	22.8	1.015	1.429	1.83	0
87	0.07	0.79	23.0	1.013	1.430	2.37	0.12
106	0.125	1.54	23.2	1.011	1.431	4.64	0.38
65	0.25	2.08	24.4	1.002	1.436	6.28	1.55
81	0.25	1.51	24.1	1.004	1.435	4.56	1.55
82	0.25	1.08	24.0	1.005	1.434	3.26	1.55
86	0.25	1.50	24.1	1.004	1.435	4.53	1.55
77	0.50	0.78	24.7	1.000	1.437	2.35	6.24
103	0.50	1.54	24.9	0.999	1.438	4.66	6.26
115	0.50	0.78	24.7	1.000	1.437	2.36	6.24
52	0.50	2.24	25.2	0.997	1.439	6.77	6.28
69	0.75	0.62	24.0	1.005	1.434	1.87	13.9
107	0.75	1.51	25.4	0.996	1.440	4.56	14.2
38	1.0	1.51	23.9	1.006	1.434	4.56	24.7
104	1.0	1.55	23.9	1.006	1.434	4.68	24.7
120	1.0	1.50	23.9	1.006	1.434	4.53	24.7

TABLE 1. Experimental parameters

The Taylor number Ta was varied over the range 10^9–10^{11}. The position of the turbulent–non-turbulent interface was monitored using a rake of thermistors arranged in the form of a helix (figure 2). The thermistors were sequentially attached to a vertical rod of 0.5 cm diameter with a clockwise angular separation of 26.5° and a vertical separation of 3 cm. This arrangement minimized the interference of the wake of a given probe with its neighbours. Because measurements were made at only a single location, and because the turbulent–non-turbulent interface was not strictly planar, some ambiguities of the time of arrival of the mean interface is encountered with this technique. It was expected, however, that a large number of data sets

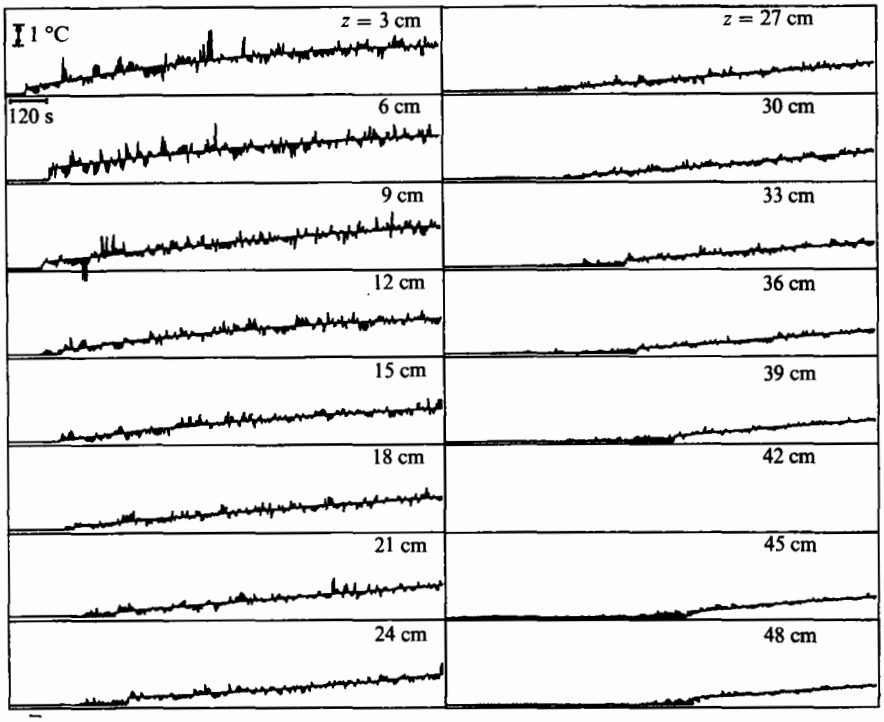

FIGURE 3. Typical temperature–time records registered by the thermistor array for run number 5; for experimental parameters see table 1. The height of the thermistors z from the base plate and the scales of the plots are also indicated. The thermistor at $z = 42$ cm was inoperable.

obtained under varying conditions, in an averaged sense, would give information on the power law for the time growth of the mixed layer.

The temperature data of each thermistor were digitized at an average rate of 5.7 Hz (multiplexed) and were stored in a microcomputer. Since the microcomputer itself was mounted on the turntable, the temperature signals could be directly transmitted to the data acquisition system without passing through potentially noisy slip rings. A typical temperature–time record of a thermistor is shown in figure 3. The time at which the temperature reading indicated a 0.2 °C increase from its original value was considered as the time of arrival of the temperature front. Temperature readings were continuously recorded and were used to calculate r.m.s. fluctuations and frequency spectra of temperature fluctuations in the mixed layer. For these calculations, only data taken after the entire fluid column became turbulent were used.

Horizontal (vertical) sheets of light 0.8 cm thick were directed through the tank at various heights (vertical planes). Particle-streak photography was used to obtain instantaneous velocity distributions in horizontal (vertical) planes. These were used to calculate r.m.s. horizontal $(\overline{u'^2})^{\frac{1}{2}}$ and vertical $(\overline{w'^2})^{\frac{1}{2}}$ velocities. Horizontal homogeneity was assumed in the calculation of $(\overline{u'^2})^{\frac{1}{2}}$. The typical number of streaks included in the horizontal velocity calculations (for a given frame) was about one hundred.

In contrast, the flow was not homogeneous in vertical planes. Thus, in calculating vertical r.m.s. velocities at a particular height from the base of the water column z, streaks that lay within a band of $z \pm 1.5$ cm, were used. Typically from 15 to 25 streaks from a given frame were included in these calculations, but occasionally

about 50 streaks could be extracted. Because the fluid column was fully turbulent, about ten frames taken successively were used for r.m.s. velocity calculations.

One difficulty in using particle streak photography is that some particles will enter and others will leave the illuminated region during the time exposure process. To overcome this problem, the light beam was 'chopped' several times during the exposure interval and the streaks that did not exhibit the required number of interruptions were disregarded. Further, chopping was done in particular patterns thus enabling the determination of flow direction.

The calculation of various system parameters was done using standard techniques. Fast-Fourier transform algorithms were used for the spectral calculations. The buoyancy b was determined using $b = g\alpha(T - T_m)$, where T is the temperature and T_m the mean temperature of the mixed layer. The change in T with time caused difficulties in calculating the r.m.s. buoyancy fluctuations $(\overline{b'^2})^{\frac{1}{2}}$. Hence T versus t plots for each thermistor were polynomial curve-fitted and departures from this mean temperature $\bar{T}(z,t)$-curve were considered as fluctuations. The estimated experimental errors were: r.m.s. horizontal velocity $\pm 5\%$, r.m.s. vertical velocity $\pm 15\%$, height ± 1 mm, time ± 2 s and temperature, ± 0.03 K.

3. Experimental results – non-rotating case

As discussed before, when the temperature difference between the water surface and ambient air is small, the upper boundary can be assumed to be insulated and, owing to the accumulation of heat, the temperature within the fluid rises slowly with time t. Thus the problem is strictly an unsteady one, but 'quasi' steady conditions can be shown to exist (Adrian *et al.* 1986) provided that the mean temperature increases at a steady rate given by

$$\bar{T}(z,t) = \overline{T_s}(z) + \overline{T_m}(t) \tag{2}$$

and that the Prandtl number Pr is independent of the mean temperature. Because the rise of T during the present experiments is small, the variation of Pr is negligible. When (2) is satisfied, the only effect of unsteadiness is the constant warming of the fluid layer and this has no dynamical influence on the turbulence field itself.

Two types of scaling have been adopted for fully developed convective turbulence. The scaling introduced by Townsend (1959) is applicable in the vicinity of the conduction layer near the boundary, where vertical motions 'feel the walls'. Since the conduction layer is much thinner than the thickness of the fluid layer H, the latter is considered to be unimportant in the wall layer. The pertinent governing parameters in this region are k_T, ν, αg and q_0; the relevant velocity, w_0, length, z_0, and buoyancy, b_0, scales thus become $w_0 = (q_0 k_T)^{\frac{1}{4}}$, $z_0 = k_T/w_0$ and $b_0 = q_0/w_0$, respectively. On the other hand, away from the conducting boundaries, in the central convective core, the heat is transported mainly by turbulence and hence the integral properties become independent of k_T. Atmospheric observations (Kaimal *et al.* 1976) and numerical simulations (Deardorff 1970*a*, *b*) clearly indicate that in this region H is the only important lengthscale. These studies further demonstrate that the relevant velocity, length and buoyancy scales in the core are $w_* = (q_0 H)^{\frac{1}{3}}$, $z_* = H$ and $b_* = q_0/w_*$, respectively.

In what follows, the observations and measurements of the non-rotating thermal convection experiments are described and comparisons are made with the predictions based on scaling arguments. Since the bulk of measurements have been made away from the conduction layer, free-convection scaling based on w_*, z_* and b_* is adopted.

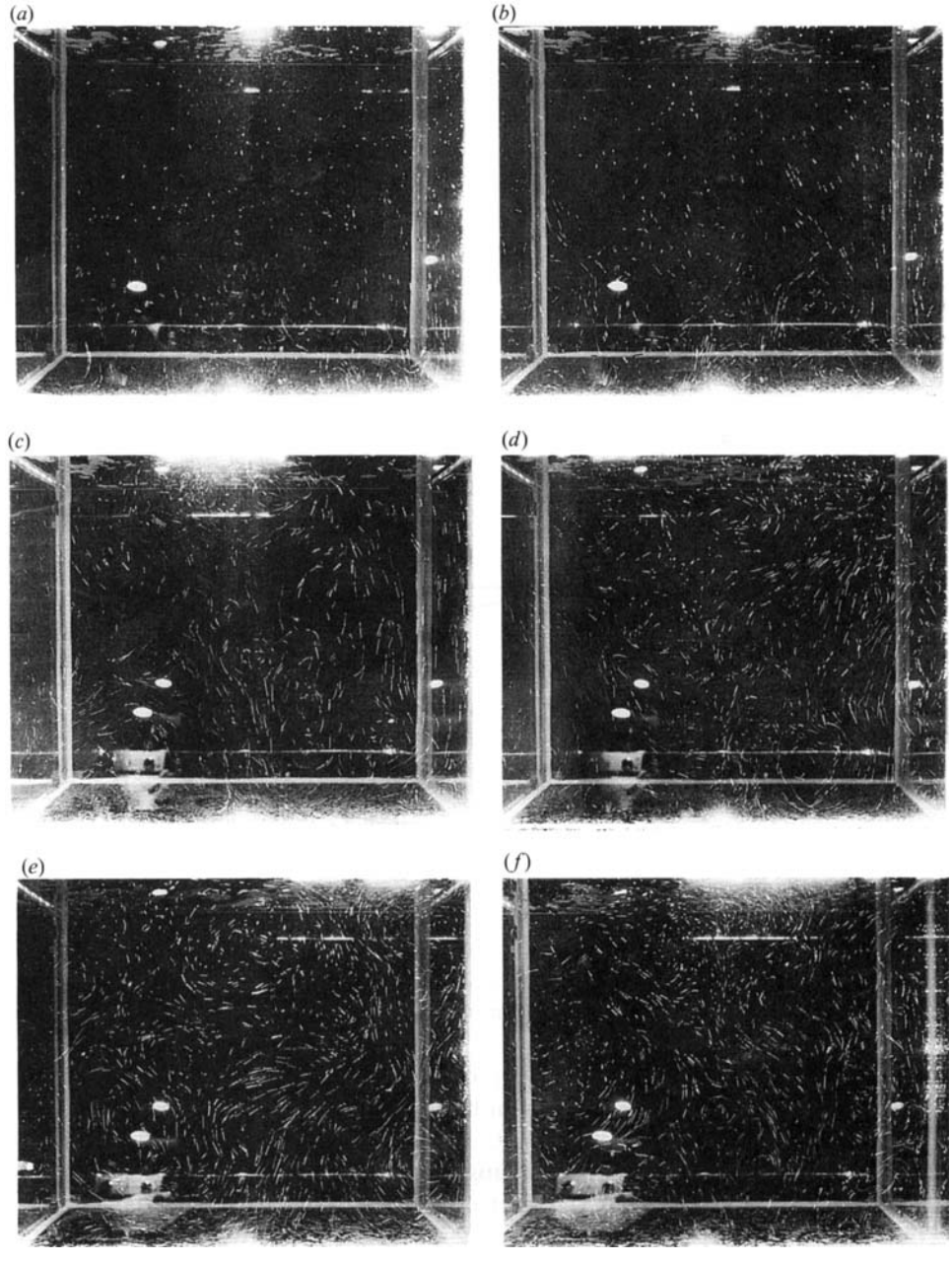

FIGURE 4. A sequence of particle-streak photographs in a vertical plane at the test-cell centre during the evolution of the convective mixed layer for a non-rotating experiment (run number 66); the times are (*a*) $t = 120$ s, (*b*) 150 s, (*c*) 210 s, (*d*) 240 s, (*e*) 960 s, (*f*) 1200 s. The exposure time was 3 s and the direction of motion is from short dash to long dash. See table 1 for experimental parameters. The dimensions of the photographs are 60×50 cm.

3.1. *Qualitative observations*

Figure 4 shows a time sequence of particle-streak photographs taken in a vertical section through the centre of the test cell and depicting the evolution of the turbulent mixed layer. As one can note, the mixed layer propagates rapidly and within three

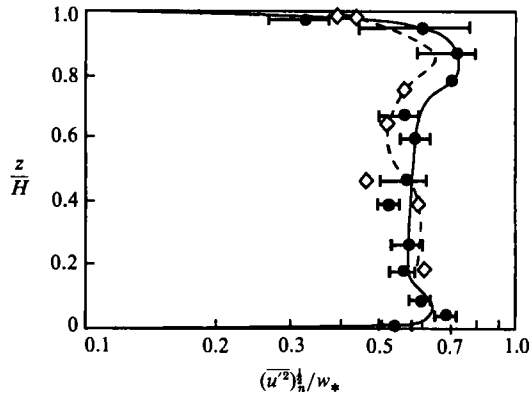

FIGURE 5. Variation of the normalized r.m.s. horizontal velocity with normalized height. The present data, denoted by ●, represent the average of experimental runs 33, 60, 64 and 66. The error bars denote the standard deviation. Solid line, LDV data of Adrian *et al.* (1986); dashed line, curve through the hot-film data of Deardorff & Willis (1985); and ◇, actual data points of Deardorff & Willis (1985).

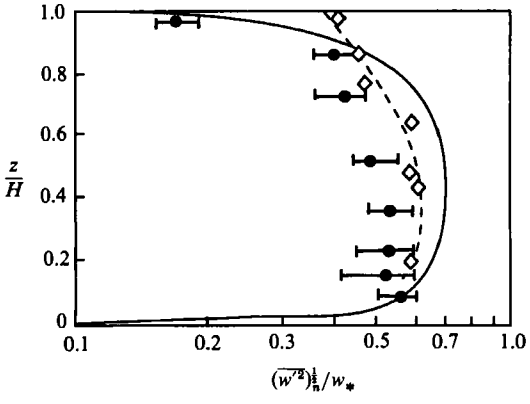

FIGURE 6. Same as figure 5, except here the normalized r.m.s. vertical velocities are plotted against the normalized height.

to four minutes the entire fluid column becomes turbulent; see figure 4(*d*). The growth rate of convective mixed layers in homogeneous fluids has been discussed in more detail by Fernando *et al.* (1989). As is evident from figure 4(*c–f*), the convection patterns change with time. Irregular, rising and sinking fluid motions are apparent on the photographs at least near the heating surface. Detailed visualization studies show that the area occupied by the hot rising fluid elements is much smaller than the area of the sinking fluid motions.

Below, we will discuss turbulence measurements in the fluid column after the turbulence fills the entire tank; see figure 4(*d–f*). We will then present measurements on the turbulence in the growing mixed layer corresponding, for example, to the experiment depicted in figure 4(*a–c*).

3.2. *Measurement of r.m.s. velocities – mixed layer throughout the fluid column*

Measurements were made of r.m.s. velocity components in non-rotating experiments in order to establish a base for comparison with their rotating counterparts. In addition, comparison with measurements of other researchers is useful in establishing

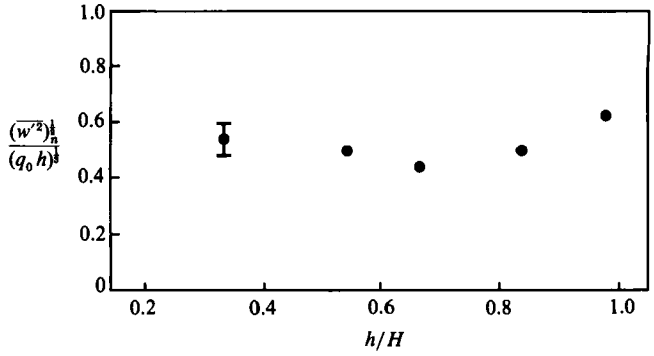

FIGURE 7. Normalized r.m.s. vertical velocities in a growing mixed layer against the normalized mixed-layer height.

confidence in the experimental techniques used in the present study. Figures 5 and 6 show the r.m.s. horizontal $(\overline{u'^2})_n^{\frac{1}{2}}$ and vertical $(\overline{w'^2})_n^{\frac{1}{2}}$ velocities, respectively, measured at various heights z from the heating surface; the subscript n indicates that the measurements are for non-rotating experiments.

Also shown on figures 5 and 6 are recent laboratory results of Deardorff & Willis (1985) and Adrian *et al.* (1986) in which hot-film anemometer and laser-Doppler velocimeter measurements, respectively, were made. Note the good agreement between these measurements and those of the present investigation, especially for the $(\overline{u'^2})_n^{\frac{1}{2}}$ component. The discrepancies observed for the vertical component may be due to sampling difficulties (§2). Although different upper boundary conditions were employed in the various experiments mentioned above, the r.m.s. velocity measurements appear to be in good agreement for all cases, indicating that the nature of the boundaries is unimportant in the core region.

3.3. *Measurements of r.m.s. velocities – growing turbulent layer*

Fernando *et al.* (1989) have shown, with experimental evidence, that the growth law for a growing convective boundary layer in a non-rotating fluid can be written as

$$h \approx 0.3(q_0 t^3)^{\frac{1}{2}}, \tag{3}$$

where h is the mixed-layer height. Relation (3) was obtained by assuming that the mechanism of the mixed-layer growth is the engulfment of non-turbulent fluid by eddies; i.e. $\mathrm{d}h/\mathrm{d}t \sim (\overline{w'^2})_n^{\frac{1}{2}}$. Furthermore the r.m.s. vertical velocity near the entrainment interface can be written in the form $(\overline{w'^2})_n^{\frac{1}{2}} \sim (q_0 h)^{\frac{1}{3}}$, where we have assumed that h for the growing mixed layer plays the same role as H when the mixed layer fills the entire fluid column.

It is not clear, however, that the scaling for $(\overline{w'^2})_n^{\frac{1}{2}}$ in a growing boundary layer can be written as $(\overline{w'^2})_n^{\frac{1}{2}} \sim (q_0 h)^{\frac{1}{3}}$, analogous to $(\overline{w'^2})_n^{\frac{1}{2}} \sim (q_0 H)^{\frac{1}{3}}$ for a turbulent column filling the entire fluid depth. In the present experiments, particle streak photographs were taken during the boundary-layer growth phase, $h < H$, using a vertical sheet of light. The $(\overline{w'^2})_n^{\frac{1}{2}}$ so obtained and scaled with $(q_0 h)^{\frac{1}{3}}$ are depicted in figure 7. In these calculations, the particle streaks lying in the region $0.2h < z < 0.8h$ were used because the turbulent velocities were shown to be nearly uniform in that region (from figure 6). The data, which include different stages of the mixed-layer growth, show that the scaling $(\overline{w'^2})_n^{\frac{1}{2}} \sim (q_0 h)^{\frac{1}{3}}$ applies even for growing boundary layers. The proportionality constant, 0.5 ± 0.07 is close to the quasi-steady case shown in figure 6.

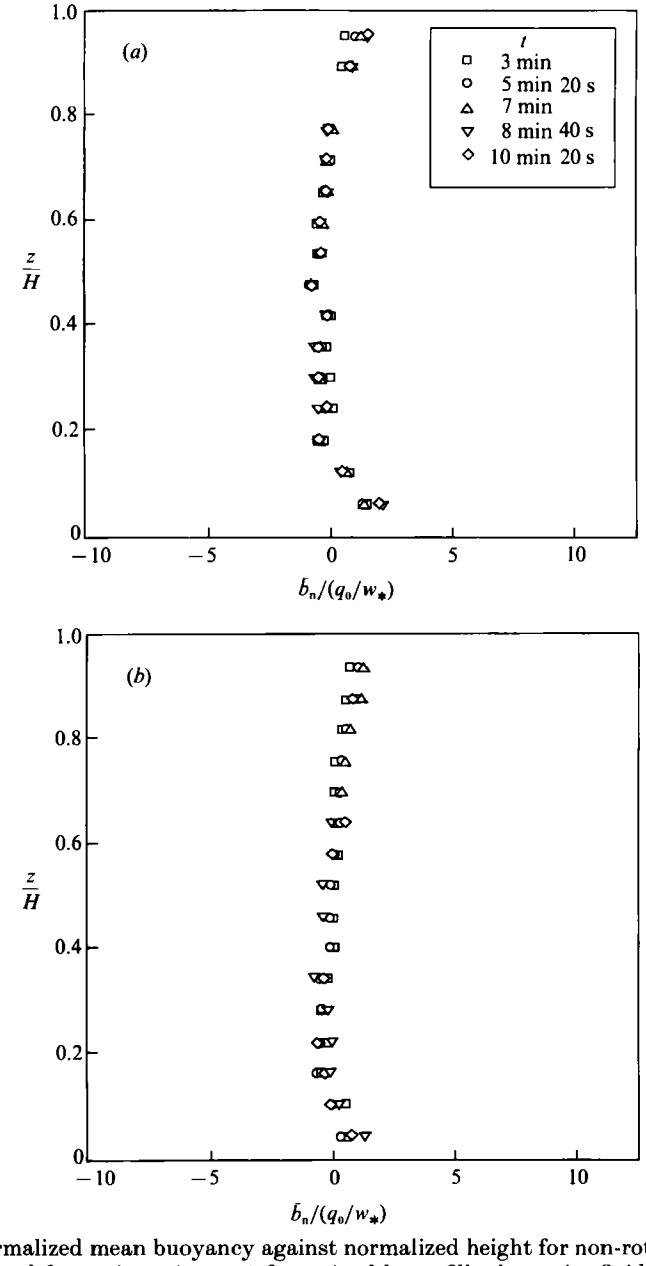

FIGURE 8. Normalized mean buoyancy against normalized height for non-rotating experiments for fixed heating and for various times t (after mixed layer fills the entire fluid column) indicated on the figure. (*a*) Run 4, (*b*) run 6.

3.4. *Measurement of mean buoyancy and r.m.s. buoyancy fluctuations*

At the start of this section, it was mentioned that the present problem becomes a quasi-steady one provided that the temperature distribution is given in the form (2). Substitution of (2) into the conservation equation for temperature

$$\frac{\partial T}{\partial t} = \frac{\partial}{\partial z}\left(k_T \frac{\partial T}{\partial z} - \overline{w'T'}\right), \tag{4}$$

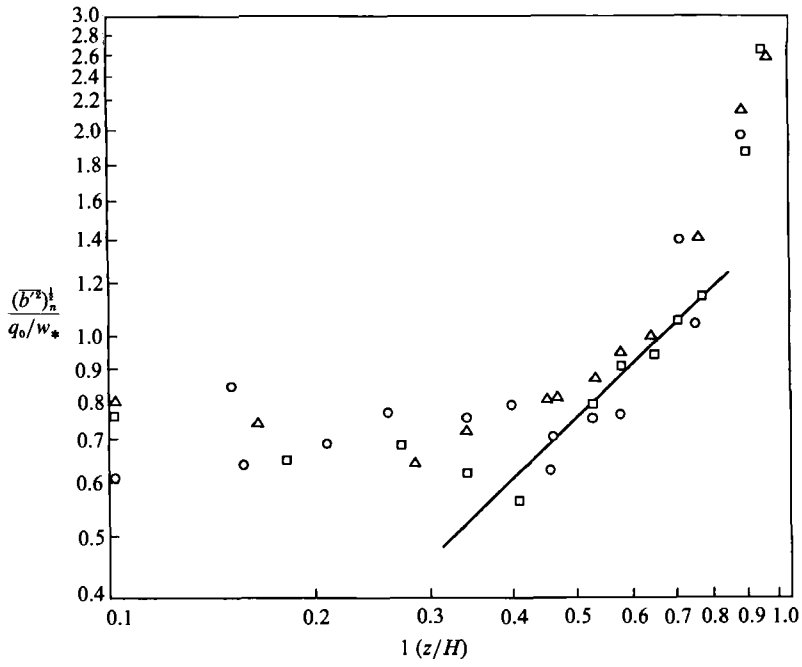

FIGURE 9. Normalized r.m.s. buoyancy fluctuations $(\overline{b'^2})_n^{\frac{1}{2}}/(q_0/w_*)$ with the complement of the normalized height $(1-z/H)$: ○, run 6; △, run 10; □, run 4.

where $\overline{w'T'}$ is the vertical temperature flux and T' is the fluctuation of temperature. Integration over the fluid column with adiabatic boundary conditions at the top surface yields

$$\dot{\bar{T}}_m = \frac{Q_0}{\rho_0 c_p H} \quad \text{or} \quad \bar{T}_m = \frac{Q_0}{\rho_0 c_p H}(t-t_0), \tag{5}$$

where t_0 is a time origin from which the temperature increments are measured. Also note that

$$\bar{T}_m = \frac{1}{H}\int_0^H \bar{T}(z,t)\,\mathrm{d}z. \tag{6}$$

Defining the mean buoyancy using $\bar{b}_n = g\alpha(\bar{T}(z,t)-\bar{T}_m(t))$, we obtain $\overline{b_n} = g\alpha\overline{T_s}(z)$, which is only z-dependent. Integration of (4), using the quasi-steady assumption, yields

$$q(z) = \overline{bw} - k_T\frac{\mathrm{d}b}{\mathrm{d}z} = q_0\left(1-\frac{z}{H}\right), \tag{7}$$

where $q(z)$ is the buoyancy flux at a given height z. For the present data sets, $\bar{T}_m$ was calculated using (6), and the mean and fluctuation of buoyancy were calculated using $\bar{b}_n = g\alpha(\bar{T}(z,t)-\overline{T_m})$ and $b' = g\alpha T'$, respectively.

Figure 8 (a, b) shows the variation of the (free-convection based) normalized mean buoyancy $\bar{b}_n(z)$ with z/H for two different experimental runs. The various symbols on each plot represent different measurement times t after the start of the experiment. We note that the excellent collapse of data on each figure supports the scaling adopted and also shows that the normalized mean buoyancy reaches a universal form (independent of time). The data on figures 8(a) and 8(b) also collapse, further supporting (5). Inspection of a large number of such plots reveals that the buoyancy

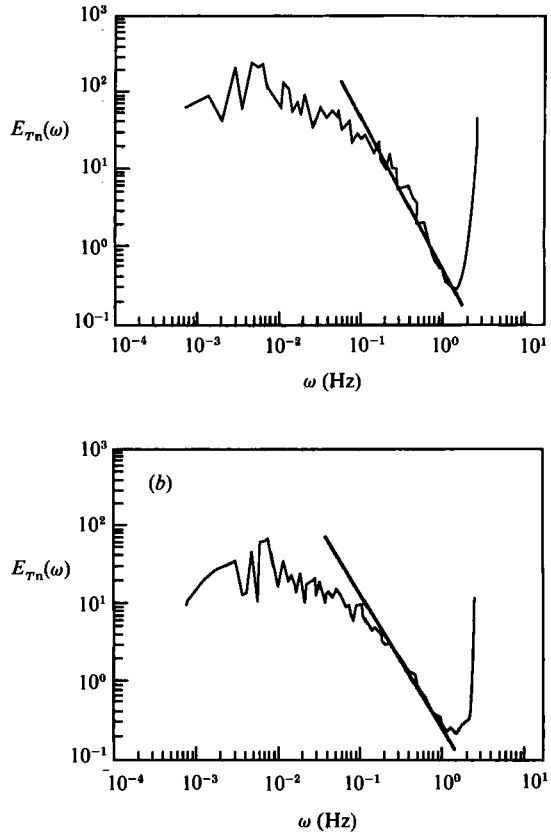

FIGURE 10. Frequency spectra obtained for non-rotating case; run number 4 at (*a*) $z = 3$ cm, (*b*) 39 cm. The solid line represents a $-\frac{5}{3}$ slope (see text).

gradient away from the boundaries, in particular at $0.35 < z/H < 0.75$, is negligible and thus, according to (7), k_T plays a minor role in the transport of heat. This observation is also consistent with that of Thomas & Townsend (1957) who found that w_0, z_0 and b_0 are only the proper scaling parameters for $z/H < 0.1$. When $\mathrm{d}b/\mathrm{d}z \approx 0$, from (6) it is possible to write $\overline{bw} \sim (\overline{b'^2})^{\frac{1}{2}} w_*$ (Adrian *et al.* 1986), leading to the scaling $(\overline{b'^2})^{\frac{1}{2}}/(q_0/w_*) \sim (1-z/H)$. Figure 9 shows a plot of $(\overline{b'^2})^{\frac{1}{2}}/(q_0/w_*)$ versus $(1-z/H)$ for a number of different q_0. The agreement with the proposed scaling, in the range $0.35 < z/H < 0.75$, appears to be satisfactory, thus supporting the assumptions made on the quasi-stationarity of the flow.

3.5. *Temperature fluctuation spectra*

The thermistor recordings at each height were used to construct the frequency ω (in Hz) spectra $E_{Tn}(\omega)$ for the temperature fluctuations. The spectra obtained for two z/H values are shown in figure 10. Inspection of a large number of such spectra indicates that, at least over a decade of frequency range, the spectra fall off as $\omega^{-\frac{5}{3}}$. The growing parts of the spectra at large frequencies are due to instrument and background noise and are presented only to show the limits of applicability of the spectra and frequency response characteristics.

A number of studies have been reported on the temperature fluctuation spectra of turbulent thermal convection. According to Howard (1963), at sufficiently large Rayleigh numbers, the behaviour of the convecting fluid depends on the dynamical

processes that take place in the conductive layer near the boundary. The boundary layer transports heat to the convecting layer by a recurrent sequence of events; namely, the growth of the conduction layer until it becomes unstable and releases buoyant thermals into the fluid, destruction of this layer by convective flow, the dying down of the convection and the reformation of the conduction layer by diffusion. Howard (1966) has estimated that the characteristic frequency of the release of thermals should be proportional to k_T/δ^2, where δ is the thickness of the conductive boundary layer. The experimental results of Castaing *et al.* (1989), however, do not support this point of view. The pseudo-two-dimensional nonlinear analysis of Foster (1971) supports Howard's (1963) mechanistic explanation of convection. His results suggest that, when $Ra_f > 10^7$ or so, the convection becomes intermittent with a characteristic period of $\tau \sim c_1(\nu/q_0)^{\frac{1}{2}}$, and a characteristic horizontal lengthscale between the thermals of $\lambda \approx c_2(k_T^2\nu/q_0)^{\frac{1}{4}}$. The predicted values of the constants are $c_1 \approx 14$ and $c_2 \approx 48$, which were found to be in reasonable agreement with other laboratory experiments (Foster & Waller 1985; Boubnov & Ivanov 1988; Castaing *et al.* 1989).

Boubnov & Ivanov (1988) and Boubnov & Golitsyn (1990) successfully used the timescale τ to collapse their spectral data with those of others; the power spectral density $E_{T\mathrm{n}}$ was scaled with $(\overline{T'^2})_{\mathrm{n}}$ and the frequency ω was scaled with τ^{-1}. It was suggested that the spectrum should be interpreted as a single continuous curve, rather than segments having power laws of the form $E_{T\mathrm{n}} \sim \omega^{\gamma}$ in each regime, as was done previously by Zimin & Ketov (1978); the latter workers have identified regions with $\gamma = -\frac{5}{3}$ and $\gamma = -4$ in the spectra. Boubnov & Ivanov (1988), however, did not rule out the possibility of such piecewise power-law behaviour of the spectrum at Rayleigh numbers higher than those used in their experiments viz. $3.2 \times 10^7 < Ra_f < 2.4 \times 10^{11}$.

Figure 11 (*a*, *b*) shows several scaled spectra (with $c_1 \approx 14$) obtained under different conditions. Spectra in figure 11 (*a*) are for a given q_0 and for different heights, whilst those in figure 11 (*b*) were measured at a given height for different q_0. All these spectra collapse satisfactorily, at least in a certain frequency range. It should be noted that there is a tendency of the experiments with low q_0 to depart from this typical behaviour; this aspect will be addressed in §4.3.

An alternative form of spectra can be proposed by considering the Eulerian nature of the measured frequency spectra. As pointed out by Tennekes (1975), in the absence of a mean flow such spectra are determined principally by eddies of different sizes being advected past the probe by the energy-containing eddies. The contribution from eddies that have wavenumbers between k and $\mathrm{d}k$ to the total temperature fluctuation can be estimated as

$$T'^2(k) \sim E_{T\mathrm{n}}(k)k \sim \chi\epsilon^{-\frac{1}{3}}k^{-\frac{2}{3}}, \tag{8}$$

where we have used the Obukhov–Corrsin spectral form for the inertial subrange of the wavenumber spectrum of temperature fluctuations $E_{T\mathrm{n}}(k)$; viz.

$$E_{T\mathrm{n}}(k) \sim \chi\epsilon^{-\frac{1}{3}}k^{-\frac{5}{3}}, \tag{9}$$

where χ and ϵ are dissipation rates of the temperature and turbulent kinetic energy, respectively. If the energy-containing eddies advect a smaller eddy of wavenumber k, to produce a frequency signal $\omega \sim k(\overline{u'^2})_{\mathrm{n}}^{\frac{1}{2}}$, then the resulting spectra should take the form

$$E_{T\mathrm{n}}(\omega) \sim T'^2(k)\,\omega^{-1} \tag{10}$$

or, using (8),

$$E_{T\mathrm{n}}(\omega) \sim \chi\epsilon^{-\frac{1}{3}}(\overline{u'^2})_{\mathrm{n}}^{\frac{1}{3}}\,\omega^{-\frac{5}{3}}. \tag{11}$$

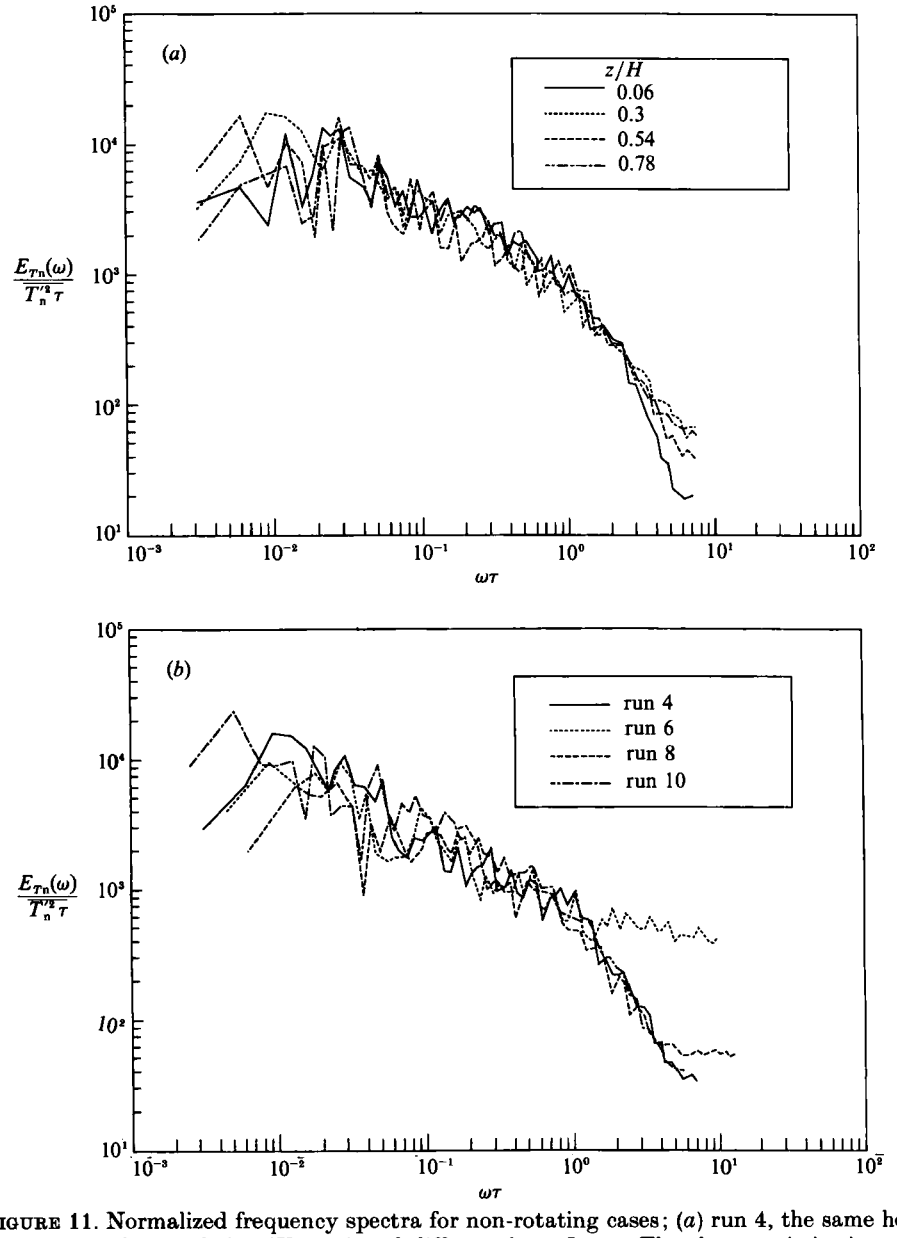

FIGURE 11. Normalized frequency spectra for non-rotating cases; (*a*) run 4, the same heating and different heights, and (*b*) $z/H = 0.3$ and different heat fluxes. The characteristic timescale of the thermals emerging from the conductive boundary layer τ has been used for the normalization. Note that the normalized E_{T_n} values have been multiplied by $2^{12}(= 4096)$.

Assuming that $\chi \sim (\overline{T'^2})_n (\overline{u'^2})_n^{\frac{1}{2}}/l$, $(\overline{u'^2})_n \sim (q_0 H)^{\frac{2}{3}}$ and $l \sim H$, we obtain, from (11),

$$\frac{E_{Tn}(\omega)}{(\overline{T'^2})_n \left(\frac{H^2}{q_0}\right)^{\frac{1}{3}}} = \alpha_1 \left[\omega \left(\frac{H^2}{q_0}\right)^{\frac{1}{3}}\right]^{-\frac{5}{3}}, \tag{12}$$

where henceforth $\alpha_1, \alpha_2, \ldots$ are used to denote constants, when the Reynolds number of turbulence is sufficiently high. The spectra presented in figure 11(*a*, *b*) are replotted in figure 12(*a*, *b*), using the new scaling given in (12). The collapse of the

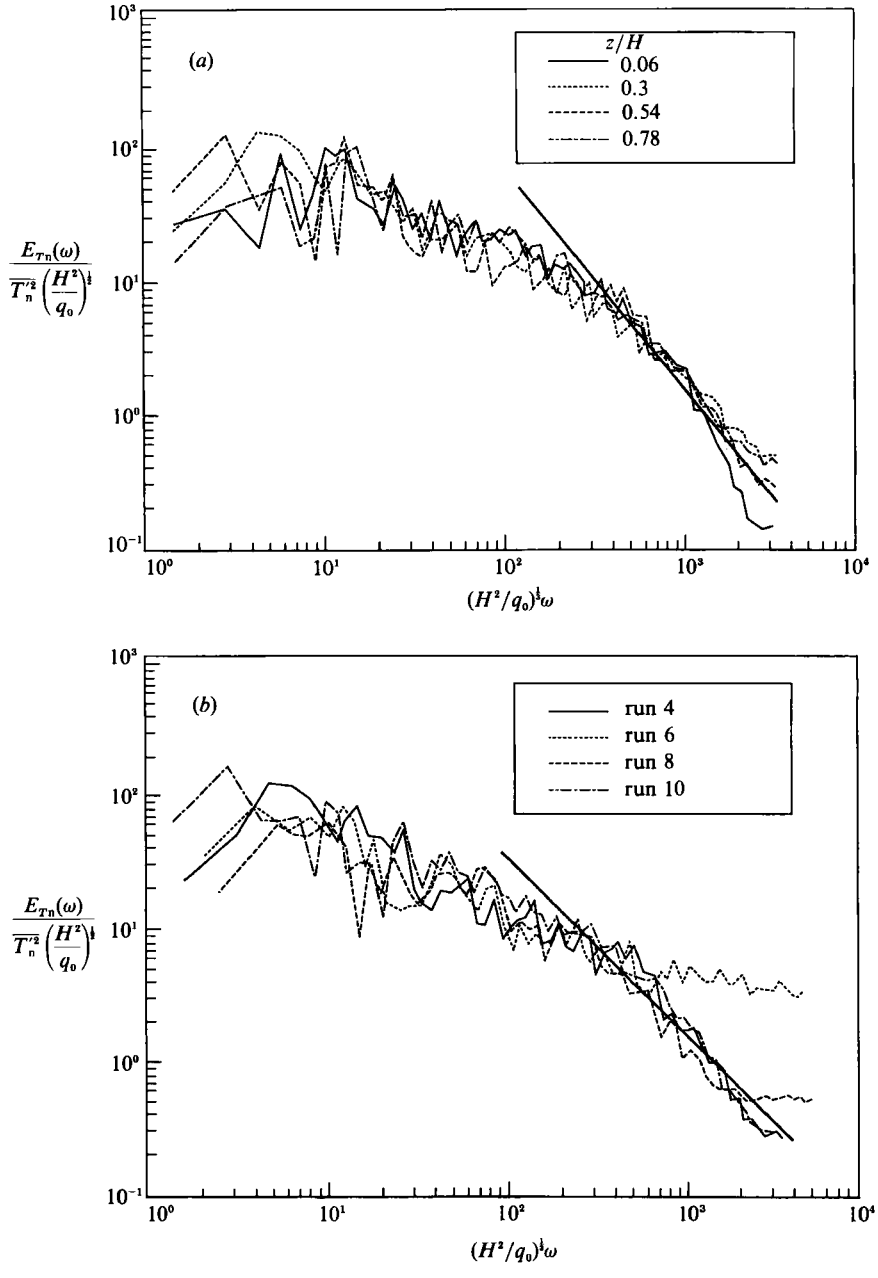

FIGURE 12. Same as figure 11, but the normalization has been done using the eddy-turnover timescale $(H^2/q_0)^{\frac{1}{3}}$ within the mixed layer. Note that the normalized E_{T_n} values have been multiplied by $2^{12}(=4096)$.

spectra is satisfactory within the measurement errors, and a $\omega^{-\frac{5}{3}}$ spectral slope can also be identified, at least over a decade of the frequency range. Note that (12) is valid only in the high-frequency range where inertial-subrange scaling is applicable. From the present measurements it is difficult to deduce which scaling is more suitable; it is hoped that future studies will be able to delineate the appropriate scaling parameters.

4. Experimental results – rotating case

4.1. *Qualitative observations*

As pointed out by Fernando *et al.* (1989), the growth of the convective mixed layer in a rotating fluid is much slower than that in the non-rotating case. Thermistor records indicate that the rotation influences the mixed-layer growth from the height of the lowest thermistor implying that, for the present experiments, the rotational effects have become important quite early in the evolution of the mixed layer; this observation is discussed further in §4.3. The observations made using horizontal light sheets show the existence of isolated, spatially and temporally varying random vortices, whose direction of rotation coincides with that of the tank and which are embedded in an otherwise turbulent fluid (figure 13). The distribution of these vortices in the horizontal plane was found to be rather inhomogeneous.

Figure 13(*a*) (i–iii) depicts a series of horizontal photographs for fixed bottom heating q_0, observation height z and observation time t, but with increasing rotation rate. The number of observed vortices appears to be increasing with Ω.

Figure 13(*b*) (i–iii) shows a series of streak photographs for fixed Ω, z and t but variable (increasing) q_0. Observations made with numerous such photographs suggest that the number of vortices is relatively independent of q_0. Figure 13(*c*) is a short-time-exposure photograph taken at an oblique angle to the tank and demonstrates that the intense vortices do not extend to the full depth of the fluid column.

The vortices form sporadically, abide for some time (typically 10–40 inertial periods) and then fade away. The velocities within the vortices are higher than the ambient turbulent velocity in the tank, and in calculating r.m.s. velocities it was necessary to adopt two sampling procedures. In one method only random convecting motions were considered whereas in the other, both random and intensely organized motions of the vortices were included. In identifying the intense vortices, the subjective judgment of the authors had to be used. For each photograph, the vortices were identified independently by each of the authors and were compared; the judgments were found to be reasonably consistent.

Motivated by the supposition of a possible relationship between the dust/steam devils observed in the lower atmosphere near the ground/above lakes, measurements were made on the physical characteristics of these vortices. The number of vortices per unit area n, maximum velocity U and the diameter D of the streamline corresponding to U (defined as the diameter of the vortex) were measured. The results indicate that $n \approx 3.8 \times 10^{-5}(\Omega/k_T)$, $D \approx 18(\nu/\Omega)^{\frac{1}{3}}$ and $U \approx 1.2(q_0/\Omega)^{\frac{1}{3}}Pr$. These measurements were found to give fair estimates for the atmospheric dust/steam devils, and a detailed account of this work is given in a separate communication (Chen, Fernando & Boyer 1989).

Although the measurements made in the present study are not detailed enough to delineate the exact formation mechanism and the dynamics of isolated vortices, it is of interest to discuss some possible evolutionary scenarios of the vortices. A plausible mechanism can be proposed based on the nature of the instabilities that develop at the conduction layer near the heated surface. As discussed above, the breakdown of this layer causes the intermittent generation of thermals. Linear stability theory (Chandrasekhar 1961) predicts that the conduction layer becomes unstable when its buoyancy gradient becomes $(\mathrm{d}b/\mathrm{d}z)_c \sim (\Omega^4 k_T^3/\delta^4\nu)^{\frac{1}{3}}$, where the proportionality constant depends slightly on the type of boundary conditions used. Because $q_0 = k_T(\mathrm{d}b/\mathrm{d}z)_c$, we obtain $\delta \sim (\Omega^4 k_T^6/\nu q_0^3)^{\frac{1}{4}}$. Further, the minimum unstable wavenumber

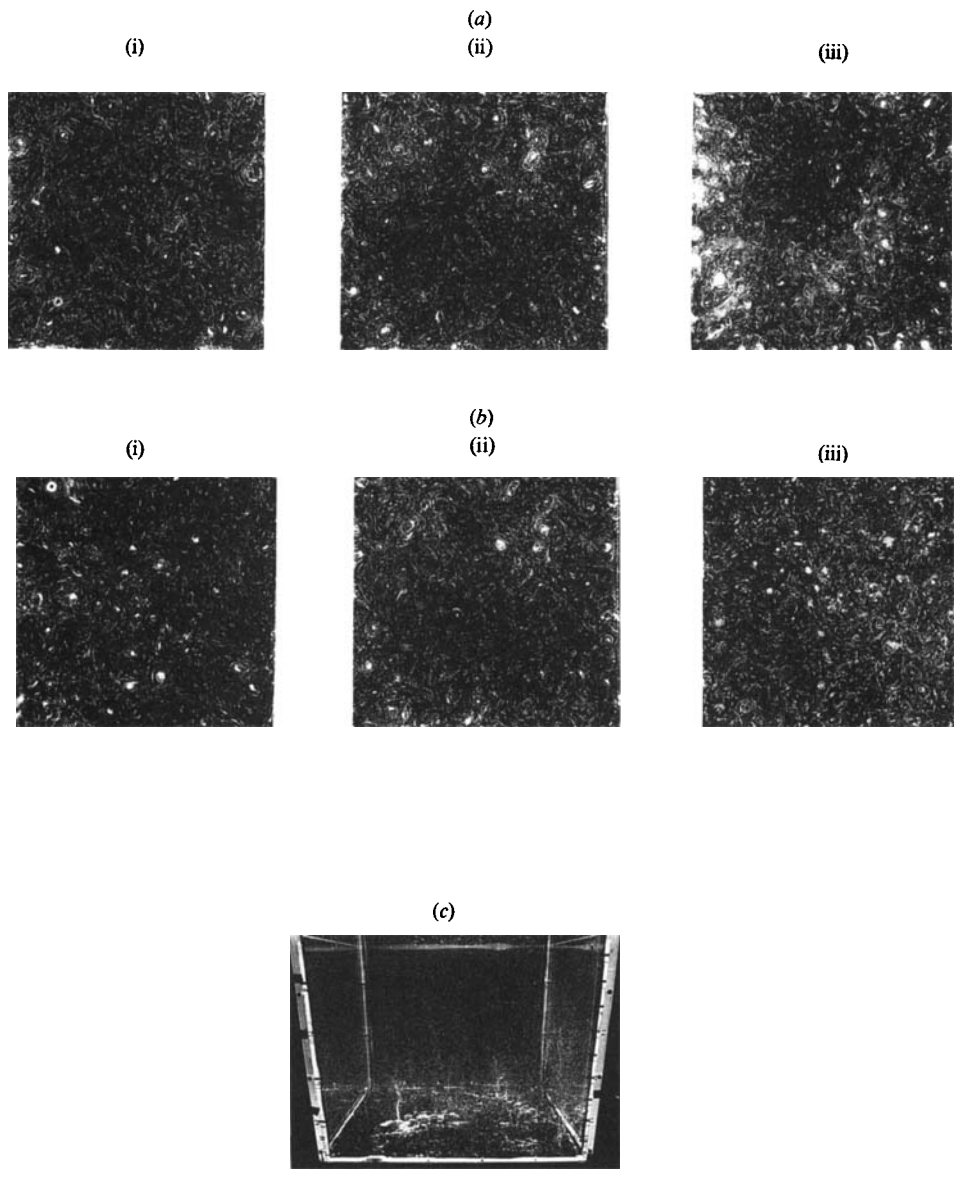

FIGURE 13. Formation of intense vortices in a rotating turbulent convecting fluid. The dimensions of the photographs are 60×60 cm for (a, b) and 60×50 cm for (c). The experimental conditions are: (a) $q_0 \approx 1.5 \times 10^{-6}$ m s^{-2}, $t = 240$ s, $z = 2$ cm and (i) $\Omega = 0.25$ (rad s^{-1}), (ii) 0.5, (iii) 1.0. (b) $\Omega = 0.5$, $t = 240$, $z = 2$ and (i) $q_0 = 7.8 \times 10^{-7}$, (ii) 1.15×10^{-6}, (iii) 1.45×10^{-6}. (c) An isometric view of height-limited intense vortices for $q_0 \approx 2 \times 10^{-6}$, $\Omega = 0.25$, $t = 240$.

at the conduction layer is given by $k \sim \delta^{-1}(\Omega^2\lambda^4/\nu^2)^{\frac{1}{6}}$ or $\lambda \sim k^{-1} \sim (\nu k_T^2/q_0)^{\frac{1}{4}}$, where λ is the wavelength of the instabilities, which can be considered as the separation scale between the vortices. Vorticity associated with these rising thermals can be amplified by stretching and can appear as intense vortices. The measured spacing between the vortices, however, does not provide support for this scaling. Alternatively, it is possible to surmise that the vortex generation process is strongly influenced by the turbulence in the convecting layer. As pointed out by Adrian *et al.* (1986), once the turbulent convection is established, the eddies can penetrate into the thermal

conduction layer and agitate it, thus altering the generation process of the thermals. Now the thickness of the thermal boundary layer can be estimated by considering the balance between the thickening of the conduction layer owing to diffusion as $\delta \sim (k_T t_d)^{\frac{1}{2}}$, where t_d is the diffusion time, and the erosion of it by turbulent eddies that have a timescale of Ω^{-1} (§4.2). This balance leads to $\delta \sim (k_T/\Omega)^{\frac{1}{2}}$, and it is interesting that this is the same as the observed horizontal scale of the vortices.

The fact that vortices are generated in turbulent rotating fluids has been known for a long time (McEwan 1976; Hopfinger *et al.* 1982); the general genesis mechanism of the vortices, however, has not been yet established (Hopfinger, Griffiths & Mory 1983). Nonetheless, several plausible models have been proposed to describe their formation and evolution (Lundgren 1985; Maxworthy, Hopfinger & Redekopp 1985; Mory & Caperan 1987). Apparently the first detailed study on vortex generation was due to Hopfinger *et al.* (1982), who imposed background rotation on oscillating-grid-induced, spatially decaying, shear-free turbulence. Near the grid, the turbulence is strong and the influence of rotation is unimportant. As the distance from the grid increases, the turbulence intensity decreases and the integral lengthscale l increases, thus causing the turbulent Rossby number $Ro = (\overline{u'^2})^{\frac{1}{2}}/2\Omega l$ to decrease. Hopfinger *et al.* (1982) found that the turbulence ceases to be three-dimensional when Ro drops below a critical value Ro_c; see also the recent work of Jacquin *et al.* (1990). According to Hopfinger (1987), $Ro_c \approx 0.2$, but more recent work of Fluery *et al.* (1991) shows that Ro_c can be as high as 0.36. When $Ro < Ro_c$, the turbulence becomes quasi-two-dimensional and tends to organize into coherent vortices which extend over the entire fluid layer. Measurements show that these vortices have a persistence time of approximately ten inertial periods, their density per unit area n is proportional to Ω and the characteristic distance between vortices scales with the integral lengthscale of the turbulence at the onset of rotational effects.

There are some important similarities and differences between the above-stated results and the present findings. The upward (z) variation of u and l at *small distances* from the heated plate, in the absence of rotational effects, can be approximated as $u \sim (q_0 z)^{\frac{1}{3}}$ and $l \sim z$ (Adrian *et al.* 1986) and thus Ro decreases with z as $(q_0/\Omega^3 z^2)^{\frac{1}{3}}$. It is possible to argue that when $Ro \approx Ro_c$, the turbulence is affected by the rotation and the formation of vortices is facilitated as in Hopfinger *et al.* (1982). Accordingly, rotational effects should become important at a distance given by $(q_0/\Omega^3 z^2)^{\frac{1}{3}} \approx Ro_c$ or when $z \sim (q_0/\Omega^3)^{\frac{1}{2}}$ and $(\overline{u'^2})^{\frac{1}{2}} \sim (q_0/\Omega)^{\frac{1}{2}}$. Although the experimental results support this assertion (§4.2) the spacing between the vortices does not scale with this lengthscale as in Hopfinger *et al.* (1982). Some differences can also be seen in the structure of the turbulence: in grid experiments, when $Ro < Ro_c$, the motions tend to be quasi-two-dimensional, whilst in the present case, the motions are strongly three-dimensional with sporadically appearing spatially intermittent vortices embedded within it. Further, perhaps owing to straining by the background three-dimensional motions, the vortices are torn apart, without extending even beyond half the depth of the fluid. In the grid-generated case, the vortices are reported to be fairly stable and extend to the surface of the fluid.

Finally it should be noted that, according to the classification scheme of Boubnov & Golitsyn shown in figure 1, the bulk of the present experiments fall into the category of 'geostropic turbulence'. Nonetheless, the quasi-random organized two-dimensional motions with highly nonlinear properties, characteristic of 'geostropic turbulence' (Salmon 1982), are not typically observed in our experiments. Instead, the bulk of the fluid was found to consist of random motions with spasmodic appearances of concentrated vortices.

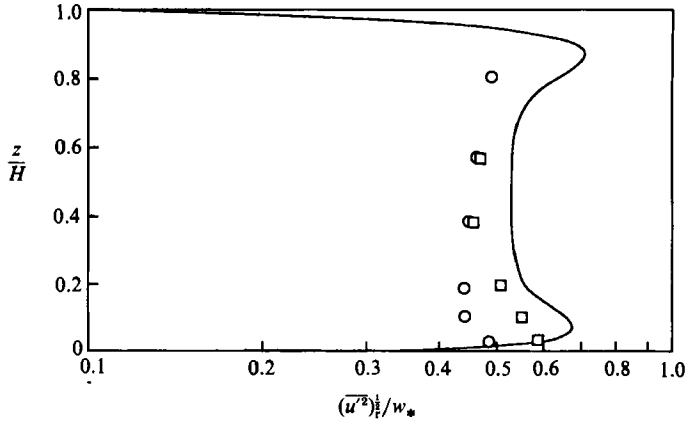

FIGURE 14. Normalized horizontal turbulent velocity against normalized height for a rotating experiment; run number 65. The solid line represents data corresponding to the non-rotating case. The r.m.s. velocities are calculated with (□) and without (○) contributions of intense vortices, respectively.

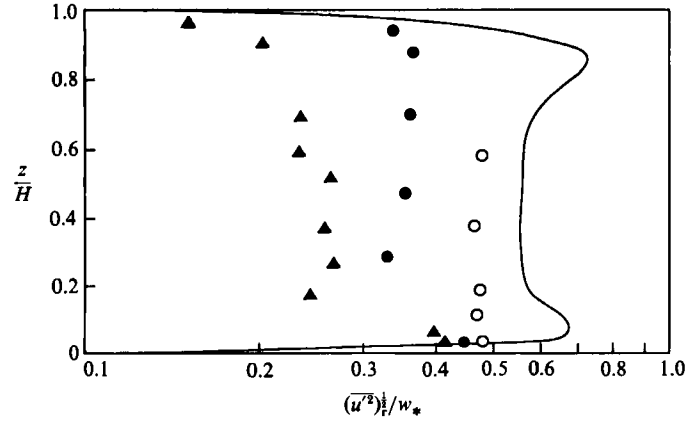

FIGURE 15. Normalized horizontal turbulent velocity with normalized height for rotating experiments; ○, $\Omega = 0.25$ rad s^{-1} (run number 82); ●, 0.5 (run number 115); and ▲, 1.0 (run number 120). Contributions from intense vortices were excluded from the calculations. The solid line represents the data corresponding to non-rotating experiments.

4.2. *Measurement of turbulence*

Figure 14 depicts the variation of the normalized horizontal turbulence intensity $(\overline{u'^2})_r^{\frac{1}{2}}/w_*$ with height z/H for a single rotating convection experiment and a comparison with its non-rotating counterpart. Henceforth the subscript r denotes quantities in the presence of rotation. As noted above $(\overline{u'^2})_r^{\frac{1}{2}}/w_*$ can be calculated in two ways; i.e. with and without considering the isolated vortices. The measurements show that at lower heights, $(\overline{u'^2})_r^{\frac{1}{2}}/w_*$ values determined including the intense vortices are higher than those without the vortices. Above the non-dimensional height $z/H \approx 0.3$, the intense vortices do not make a significant contribution to $(\overline{u'^2})_r^{\frac{1}{2}}/w_*$. Because the velocity measurements were made at discrete heights, the exact location where the vortices lose their identity could not be determined.

The effects of rotation on convective turbulence are further illustrated in figure 15 in which the height variation of $(\overline{u'^2})_r^{\frac{1}{2}}/w_*$ (excluding vortices) is presented as a

function of Ω. Inhibition of turbulence by rotation is clearly evident. Consequently, the convective turbulent boundary-layer scaling, used in §3.2, is not applicable to the rotating case and new scaling variables are needed to interpret the data. The most plausible way to deduce such scales is to assume that the lengthscale l_r in rotating turbulence is determined by a balance between the inertial forces of the eddies $(\overline{u'^2})_r/l_r$ and the associated Coriolis forces $\Omega(\overline{u'^2})_r^{\frac{1}{2}}$, viz.

$$l_r \sim \frac{(\overline{u'^2})_r^{\frac{1}{2}}}{\Omega}. \tag{13}$$

This argument is analogous to the buoyancy–inertial force argument used in stratified turbulence and has been discussed by Hopfinger *et al.* (1982), Dickinson & Long (1983), Fernando (1987*b*) and Hopfinger (1987, 1989). Thus, unlike the non-rotating case, the turbulent lengthscales are limited by constraints other than the depth of the mixed layer H, and hence H may no longer be important in determining the small-scale turbulence characteristics if $H \gg (\overline{u'^2})_r^{\frac{1}{2}}/\Omega$. Although this argument is strictly valid only for motions perpendicular to the axis of rotation (horizontal motions), experiments with oscillating-grid-induced turbulence (Dickinson & Long 1983) show a drastic change in the vertical growth characteristics after the rotational effects become important at a critical lengthscale, thus suggesting that both horizontal and vertical scales of turbulence are affected by the rotational effects almost simultaneously. Further, it has been found that beyond the lengthscale l_r, the turbulence becomes two-dimensional and the energy is transported vertically by inertial waves and vortex solitons. As mentioned in §4.1, detailed flow visualization studies show that, in the present experiments, neither regular vortex cores nor strongly two-dimensional motions are present. Perhaps this may be due to the differences in forcing; in contrast to the oscillating-grid experiments, in the convection experiments the thermal forcing causes turbulent velocities to increase with the growth of the mixed layer. Hopfinger (1987, 1989) has argued that the turbulence is affected by the rotation when the local Rossby number $Ro = (\overline{u'^2})_r^{\frac{1}{2}}/2\Omega l_r$ is of the order one and the turbulence becomes fully two-dimensional ('collapsed') when $Ro \approx 0.2$. In the present experiments $Ro \approx 0.75$ was observed (see (18) below) thereby suggesting the existence of rotationally affected, but 'non-collapsed' turbulence.

If H is unimportant, then the turbulent velocity scales and lengthscales become functions of q_0 and Ω only and thus it is possible to write, at the onset of rotational effects,

$$l_r = \alpha_2(q_0/\Omega^3)^{\frac{1}{2}} \tag{14}$$

and

$$(\overline{u'^2})_r^{\frac{1}{2}} = \alpha_3(q_0/\Omega)^{\frac{1}{2}}. \tag{15}$$

Note that (14) and (15) are the same as those obtained in §4.1 by assuming that the rotational effects become important when the local Ro falls below a critical value. Figure 16 shows height versus velocity data, normalized using the scaling (14) and (15), for several experiments. The data collapse is excellent, suggesting the validity of the proposed scaling. The value of α_3 can be estimated from the data with $z > h_c$ as $\alpha_3 = 1.70 \pm 0.14$, where h_c is the height at which the rotational effects become important.

The lengthscale at which the turbulence is affected by the rotation can be found by locating the height at which the r.m.s. velocity data depart from the non-rotating measurements: for example, see figure 15. Since data were taken at discrete heights it is not possible to locate the exact position h_c at which this departure will occur. By

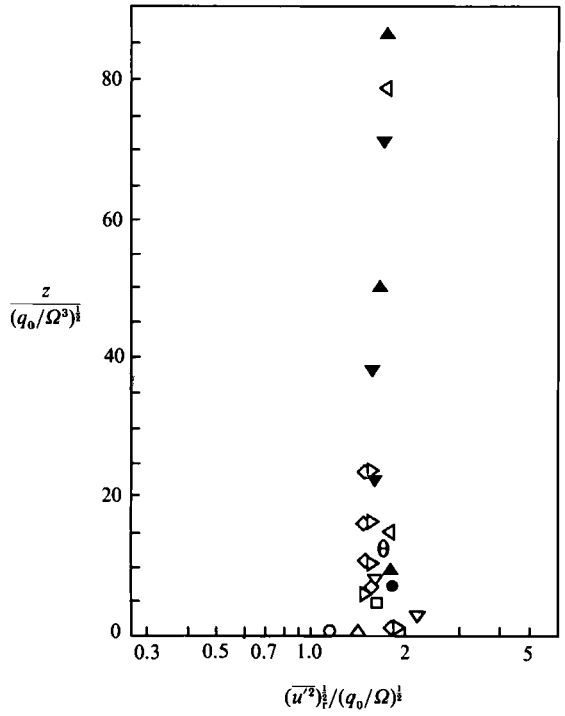

FIGURE 16. Normalized turbulent horizontal velocity $(\overline{u'^2})_r^{\frac{1}{2}}$ versus normalized height z for rotating experiments, for various heating and rotation rates: ○, run 106; ▽, run 82; ◇, run 86; ▷, run 81; △, run 87; □, run 52; ●, run 77; θ, run 107; ▲, run 115; ▼, run 120.

inspection of several experimental runs and locating the maximum $(\overline{u'^2})_r/(q_0/\Omega)^{\frac{1}{2}}$ where the $(\overline{u'^2})_r$ data agree with the non-rotating case and the minimum $(\overline{u'^2})_r/(q_0/\Omega)^{\frac{1}{2}}$ where the data agree with (15), it was possible to estimate h_c with an accuracy of $\pm 10\%$. The results show

$$h_c \approx 4.5(q_0/\Omega^3)^{\frac{1}{2}}. \tag{16}$$

Using $l_r = 0.25h_c$ (Hunt 1984), it is possible to estimate $\alpha_2 \approx 1.1$. It is interesting to note the relationship of h_c to the lengthscale $(\epsilon/\Omega^3)^{\frac{1}{2}}$, which is the rotating counterpart of the Ozmidov lengthscale commonly used in stratified turbulence. Based on the relation $\epsilon \approx 0.6q_0$ obtained in the atmospheric context (Kaimal *et al.* 1976), we may write

$$h_c \approx 5.8(\epsilon/\Omega^3)^{\frac{1}{2}} \tag{17a}$$

or

$$l_r \approx 1.5(\epsilon/\Omega^3)^{\frac{1}{2}}. \tag{17b}$$

Finally it is noted that within the rotationally affected convective core, the turbulent Rossby number is given by

$$Ro = (\overline{u'^2})_r^{\frac{1}{2}}/2\Omega l_r \approx 0.75. \tag{18}$$

It should be noted that the velocity scale $(q_0/\Omega)^{\frac{1}{2}}$ for rotating convection was first derived by Golitsyn (1980). He assumed that the flow field away from the boundaries was in geostropic equilibrium and used the energy balance for high-Nusselt-number convective turbulence in his derivation. In a later study, Golitsyn (1981), attempts have been made to experimentally determine α_3 using a Taylor's ink-wall-type experiment performed in carbonated (bubbling) water. The experimental results, when combined with an approximate energy balance, yielded $\alpha_3 \approx 2.3 \pm 0.4$, which is

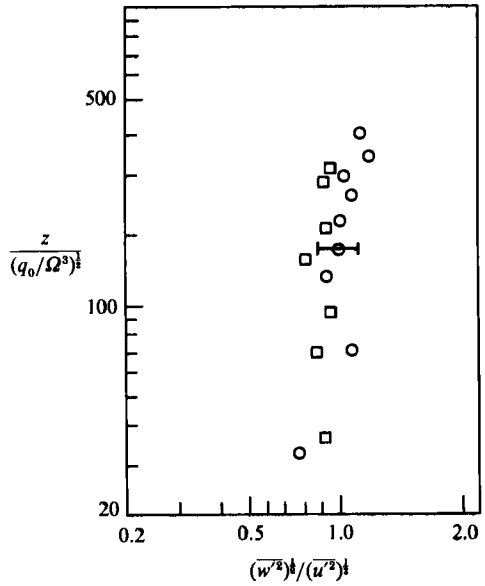

FIGURE 17. The variation of the ratio of vertical to horizontal r.m.s. velocities in rotating convection with the normalized distance from the heating surface: □, run 69; ○, run 38.

somewhat higher than that obtained from the present direct measurements. More recent measurements by Boubnov & Golitsyn (1990) have shown that α_3 should be close to 1.7.

As mentioned in §2, it was difficult to obtain sufficiently large samples of particle-streak data for the calculation of the vertical velocity component. By inspecting streak photographs, two experimental runs that contained more than fifty data points for most of the height intervals were located, from which the vertical and horizontal turbulent intensities were calculated; the ratio of r.m.s. velocities, as a function of the non-dimensional height is shown in figure 17. Note the near-isotropy of turbulence, especially in the convective core. Although it might be expected that only horizontal motions are affected by rotation, the present results show that rotational effects are immediately felt by the vertical component via inter-component turbulent energy transport.

It is of interest to note the atmospheric implications of the above results. Using the typical values $q_0 \approx 5 \times 10^{-3}$ m^2 s^{-3} and $\Omega \approx 7 \times 10^{-5}$ s^{-1} for the atmosphere (Caughey 1982), we find $h_c \approx 5.4 \times 10^5$ m (540 km). Since the maximum height of the atmospheric boundary layer is about 1–2 km, it is concluded that small-scale turbulence in the PBL is not affected by planetary rotation. This result is generally assumed in PBL studies but, to our knowledge, no systematic, controlled, laboratory experiments have previously been performed to check its validity. Numerical models designed to study the effect of rotation on small-scale PBL turbulence have not been successful in resolving this issue without contention; recent results of Stubley & Riopelle (1988) show that planetary rotation does not have a significant effect on PBL processes, whereas the computations of Detering & Etling (1985) suggest the opposite.

4.3. *Mixed-layer growth in rotating fluids*

It is of interest to study convective mixed-layer growth in the presence of rotational effects. The major difference between the rotating and non-rotating cases will be the inhibition of the development of the integral lengthscale in the former case, when

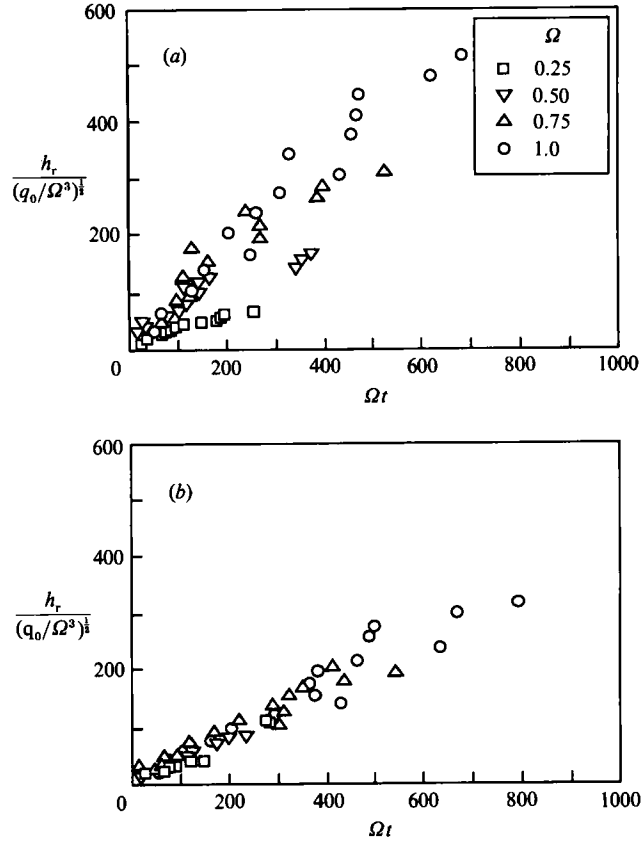

FIGURE 18. Normalized mixed-layer growth rates against normalized time for rotating flows for heat fluxes (*a*) $q_0 = 7.5 \times 10^{-7}$, (*b*) $q_0 = 2.25 \times 10^{-6}$ and for various rotations for each heat flux value. In (*a*), □, run 14; ▽, run 9; △, run 20; ○, run 15; and in (*b*), □, run 12; ▽, run 11; △, run 13; ○, run 17.

the mixed-layer height becomes $h_c \approx 4.5(q_0/\Omega^3)^{\frac{1}{2}}$. For typical experimental values, $q_0 \approx 1.5 \times 10^{-6}$ m^2 s^{-3} and $\Omega \approx 0.5$ rad s^{-1}, we find $h_c \approx 1.5$ cm; because the lowest thermistor is at $z = 3$ cm, this means, as mentioned in §4.1, that almost all of the growth data obtained during the rotating experiments include the influence of rotation.

If we assume that the mixed-layer growth occurs by the engulfment of non-turbulent fluid by turbulent eddies, it is reasonable to assume $\mathrm{d}h_r/\mathrm{d}t = \alpha_4(\overline{u'^2})_r^{\frac{1}{2}} = \alpha_3\alpha_4(q_0/\Omega)^{\frac{1}{2}}$, where we have used the fact that $(\overline{u'^2})_r^{\frac{1}{2}} \approx (\overline{w'^2})_r^{\frac{1}{2}}$ and where $(\overline{u'^2})_r^{\frac{1}{2}}$ has been obtained from (15). One can then write

$$h_r = \alpha_3\alpha_4\left(\frac{q_0}{\Omega}\right)^{\frac{1}{2}} t, \tag{19a}$$

or

$$\frac{h_r}{(q_0/\Omega^3)^{\frac{1}{2}}} = \alpha_3\alpha_4\,\Omega t. \tag{19b}$$

Figure 18(*a*, *b*) shows the comparison of (19) with the experimental results for widely differing q_0 and Ω values; note the good agreement, particularly at large q_0 values. The scatter in the low-q_0 ($\approx 7.5 \times 10^{-7}$ m^2 s^{-3}) case may be due to the

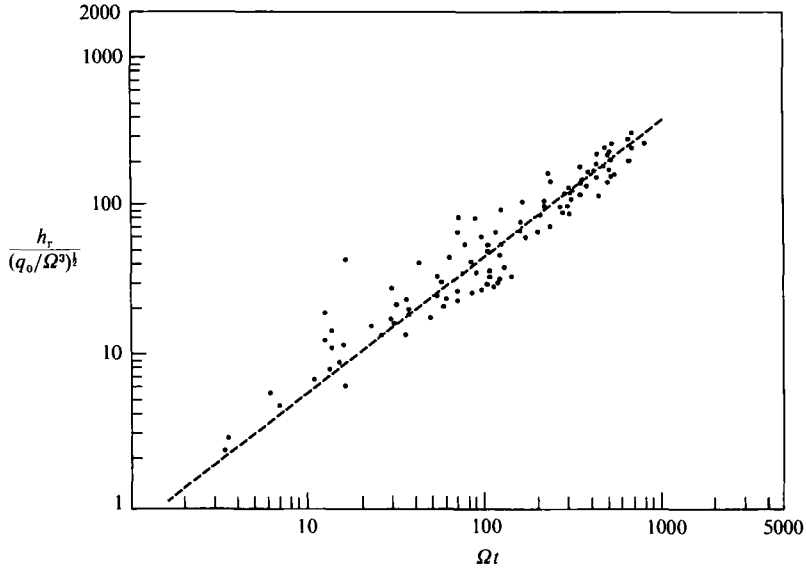

FIGURE 19. Normalized mixed-layer height against normalized time for experiments carried out with $q_0 > 1.5 \times 10^{-6}$ m^2 s^{-3}.

importance of molecular effects in thermal convection. Fernando, Muñoz & Zangrando (1988) proposed that the convective turbulence becomes influenced by viscous effects when the Reynolds number $Re = w_* H/\nu < 3600$; for the experiments pertinent to figure 18(*a*, *b*), the Reynolds numbers are 3600 and 5200, respectively. Figure 19 depicts a combined plot of eight experiments covering the range $1.5 \times 10^{-6} < q_0 < 2.25 \times 10^{-6}$ (m^2 s^{-3}) and $0.25 < \Omega < 1$ rad s^{-1}; the data from figure 17(*a*) are excluded. From figure 19 we find $\alpha_3 \alpha_4 \approx 0.7$, thus $\alpha_4 \approx 0.5$. Fernando *et al.* (1989) attempted to collapse the mixed-layer growth data by including the thermal diffusivity k_T as an important variable. By trial and error, it was found that

$$\frac{h_r}{(q_0/\Omega^3)^{\frac{1}{2}}} \approx 1.5 \Omega t G^{\frac{1}{4}}, \tag{20}$$

where $G = \Omega^2 k_T/q_0$, can collapse the data quite successfully. It is difficult to justify, however, that k_T can have a significant effect in the turbulent mixed-layer growth. Because $Pr > 1$, where Pr is the Prandtl number, the viscous effects should first play a role. On this basis, we may anticipate $h_c = h_c(q_0, \Omega, t, \nu)$ or $h_c/(q_0/\Omega^3)^{\frac{1}{2}} = f(G_1, \Omega t)$, where $G_1 = \Omega^2 \nu/q_0$. Note that since Pr is approximately a constant, an equation of the form (20), with G replaced by G_1 and the proportionality constant replaced by $1.5 Pr^{-\frac{1}{4}}$, will also give a good collapse of the data. For the convenience of comparison with figure 18, such a plot is given in figure 20. Note that the spread of data in both cases does not differ appreciably. The results suggest

$$\frac{h_r}{(q_0/\Omega^3)^{\frac{1}{2}}} \approx 0.85 \Omega t G_1^{\frac{1}{4}}, \tag{21a}$$

or

$$h_r \approx 0.85 (q_0 \nu)^{\frac{1}{4}} t. \tag{21b}$$

If it is assumed that, as in non-rotating convection, $\epsilon/q_0 \approx 0.6$, then (21*b*) becomes $h_r \approx 0.95 u_k t$, where $u_k = (\epsilon\nu)^{\frac{1}{4}}$ is Kolmogorov's velocity scale. Two theories presently

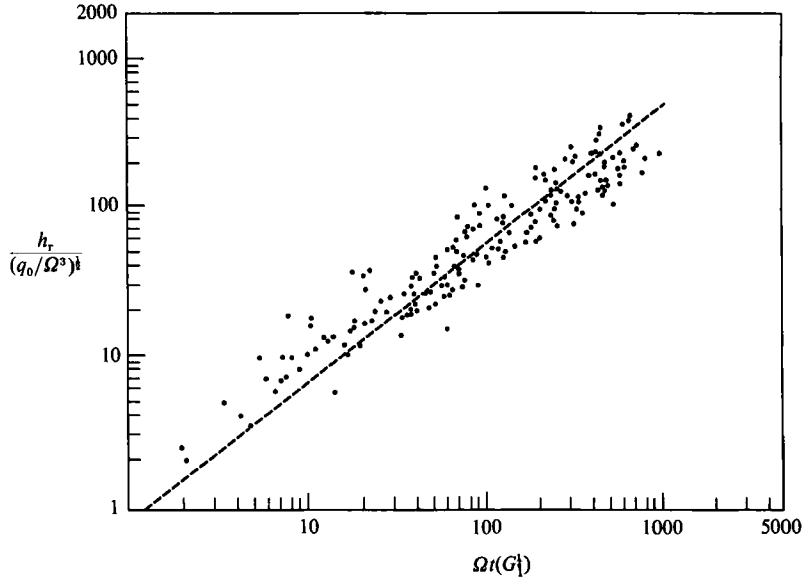

FIGURE 20. Normalized mixed-layer height against normalized time (see text).

exist pertinent to the growth of mixed layers in turbulent fluids. In the first, the engulfment of non-turbulent fluid by the energy-containing eddies is assumed whilst in the second, straining of the entrainment interface by Kolmogorov-scale eddies is assumed. Because of the satisfactory collapse of data when formulations based on both theories are tested against experimental results, it is not possible to deduce the most appropriate entrainment law from the present rotating experiments alone, but some inferences can be drawn from the results of non-rotating experiments. According to Fernando *et al.* (1989), the convective mixed-layer growth in a homogeneous non-rotating fluid follows $h \approx (q_0 t^3)^{\frac{1}{4}}$, which implies that the entrainment velocity near the interface scales with the r.m.s. velocity near the interface; because, for this case also $u_k \sim (q_0 \nu)^{\frac{1}{4}}$, a linear growth should be expected if the entrainment velocity scales with u_k. On this basis we tend to accept (19) over (21*b*).

Finally, it is important to comment on the suitability of using u_r and l_r, measured when the turbulence fills the tank, to predict the initial growth rate. At the onset of turbulence, only large scales are produced, while the smaller scales are generated later by vortex stretching mechanisms. If it is assumed that the timescale for the development of small scales is of the order of the eddy turnover timescale, l_r/u_r, it is possible to estimate the time for the development of small scales as $0.7\Omega^{-1}$. Since the bulk of the present measurements have been taken at times $\Omega t > 10$, it is assumed that the turbulence intensity during the mixed-layer growth is similar to that of fully developed turbulence.

4.4. *Measurement of mean and r.m.s. fluctuation of buoyancy*

As discussed in §4.2, the scales of turbulent motion in non-rotating and rotating cases are very different. In the former case, the size of the energy-containing eddies scales with the size of the mixed layer and, hence, scales smaller than this are expected to be well mixed. In contrast, for rotating flows, if $H \gg (q_0/\Omega^3)^{\frac{1}{4}}$, the integral scale is proportional to $(q_0/\Omega^3)^{\frac{1}{4}}$, as in the present experiments. The turbulent layer cannot then we well mixed on all scales filling the tank, thus leading to an appreciable

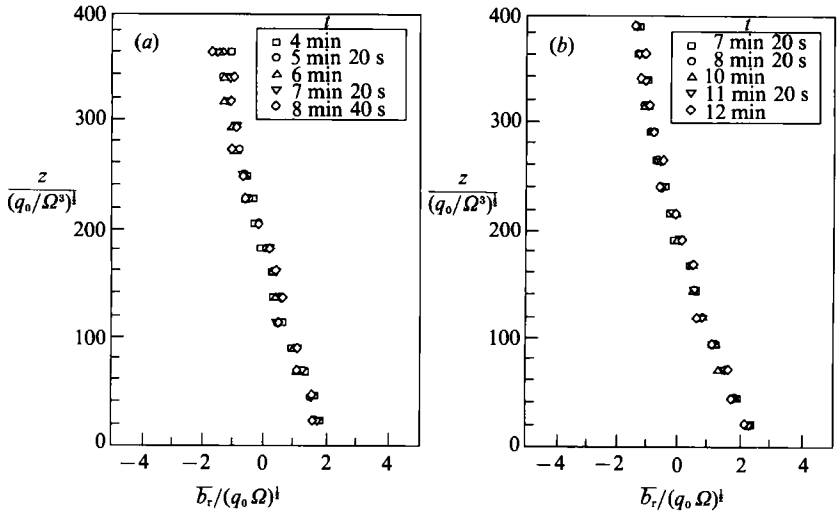

FIGURE 21. The variation of non-dimensional mean buoyancy with non-dimensional height (after the mixed layer fills the entire fluid column) for various times shown on the figure. (*a*) Run 20, (*b*) run 19.

buoyancy gradient within the turbulent layer. On dimensional grounds it is possible to write the expressions for the mean and r.m.s. fluctuation of buoyancy as

$$\bar{b}_r(z) = f_1(z, q_0, \Omega), \tag{22a}$$

or

$$\frac{\bar{b}_r(z)}{(q_0\Omega)^{\frac{1}{2}}} = f_2\left\{\frac{z}{(q_0/\Omega^3)^{\frac{1}{2}}}\right\}, \tag{22a, b}$$

and

$$\frac{(\overline{b'^2})_r^{\frac{1}{2}}}{(q_0\Omega)^{\frac{1}{2}}} = f_3\left\{\frac{z}{(q_0/\Omega^3)^{\frac{1}{2}}}\right\}, \tag{23}$$

where f_1, f_2 and f_3 are functions and it has been assumed that H is no longer a relevant parameter.

Figure 21 (*a*, *b*) shows the variation of $\bar{b}_r/(q_0\Omega)^{\frac{1}{2}}$ with $z/(q_0/\Omega^3)^{\frac{1}{2}}$ taken at different times for two different experimental runs. The excellent collapse of data supports the universal functional form (22*b*) for rotating convection. Note the presence of an appreciable buoyancy gradient within the mixed layer, compared to the non-rotating cases shown in figure 8. The buoyancy gradient within a rotating–convecting mixed layer can be estimated as $(\mathrm{d}b/\mathrm{d}z)_r \sim (\overline{b'^2})_r^{\frac{1}{2}}/l_r \sim q_0/(\overline{w'^2})_r^{\frac{1}{2}}/l_r \sim \Omega^{-2}$, whereas within the non-rotating convective mixed layer it becomes $(\mathrm{d}\bar{b}/\mathrm{d}z)_n \sim (\overline{b'^2})_n^{\frac{1}{2}}/H \sim q_0/w_*H$. The ratio of the mixed-layer buoyancy gradients within the rotating and non-rotating cases can be written as

$$\begin{aligned}(\mathrm{d}\bar{b}/\mathrm{d}z)_r/(\mathrm{d}\bar{b}/\mathrm{d}z)_n &\sim (\Omega^3H^2/q_0)^{\frac{2}{3}} \\ &\sim [H^2/(q_0\Omega^{-3})]^{\frac{2}{3}} \sim (H/h_c)^{\frac{4}{3}} \gg 1,\end{aligned} \tag{24}$$

which explains the reason for the substantial gradients observed in the mixed layer for the rotating case.

Figure 22 shows the variation of the normalized r.m.s. fluctuations in the mixed layer with the normalized height. The collapse of the data is fair and provide support for the functional form (23). It is noted that attempts made to collapse the data with

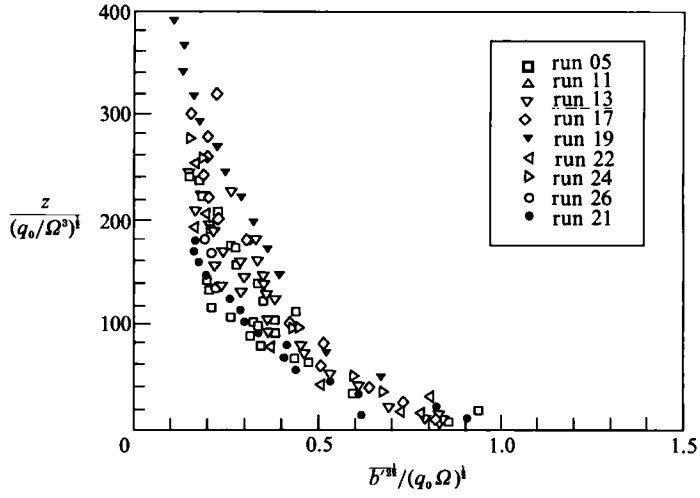

FIGURE 22. A plot of non-dimensional r.m.s. buoyancy fluctuations with non-dimensional height. Experimental run numbers are given in the legend (see table 1).

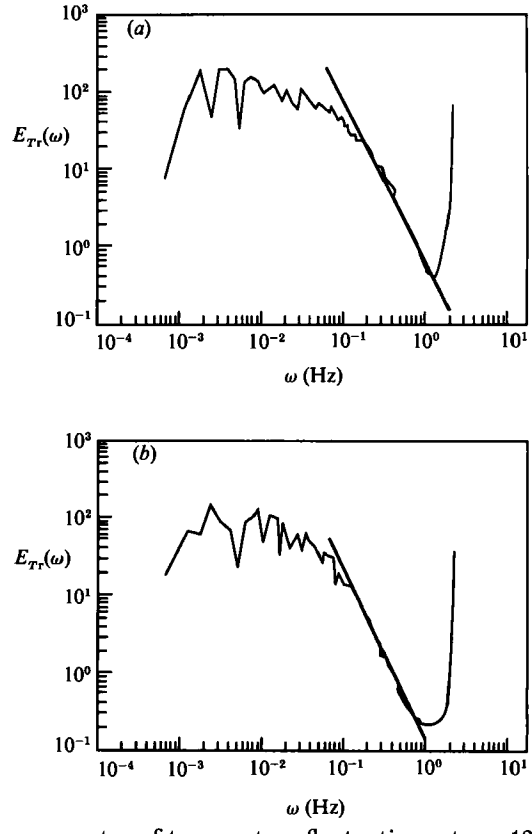

FIGURE 23. Frequency spectra of temperature fluctuations at $z = 12$ cm and for (*a*) run 11 and (*b*) run 9. Note that the normalized E_{Tn} values have been multiplied by $2^{12}(= 4096)$.

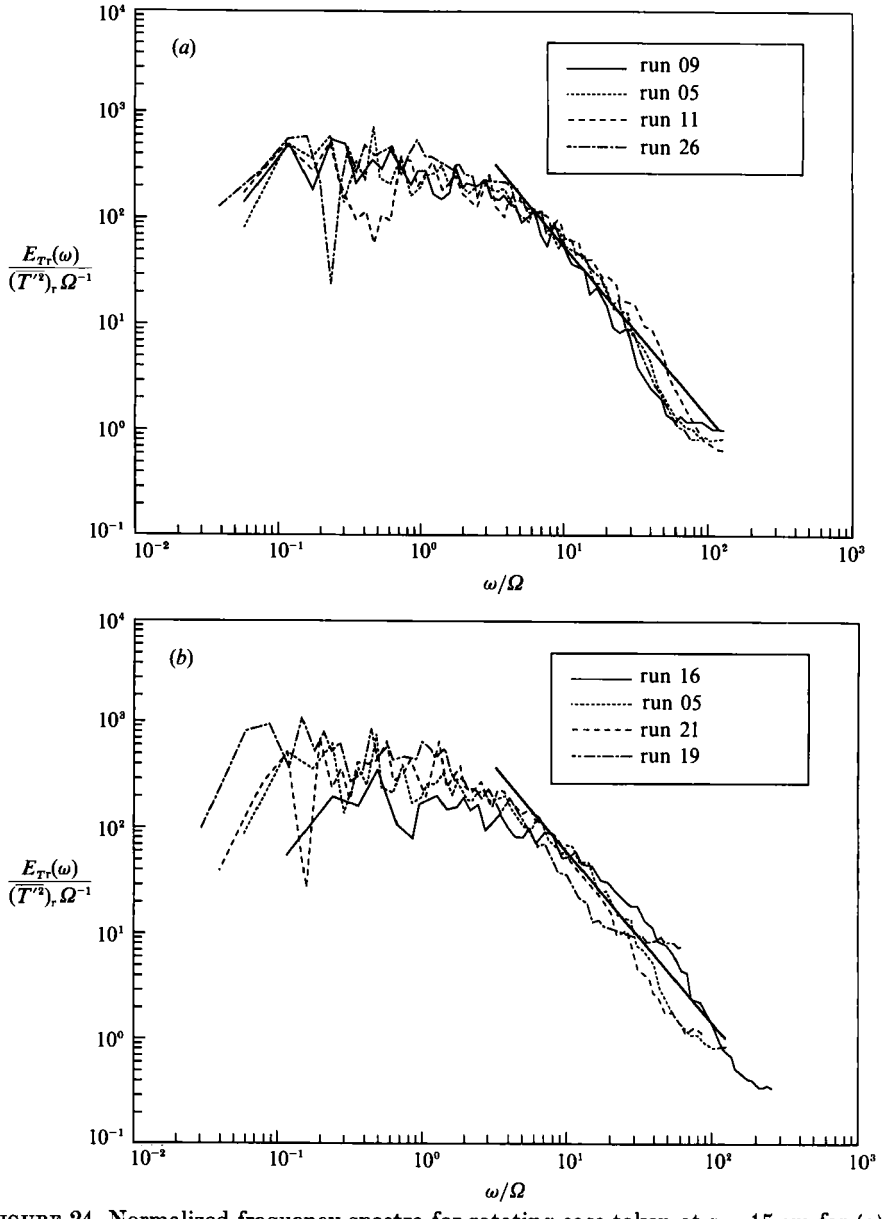

FIGURE 24. Normalized frequency spectra for rotating case taken at $z = 15$ cm for (a) constant Ω and varying q_0 and (b) approximately constant q_0 and varying Ω. Note that the normalized E_{Tn} values have been multiplied by $2^{12}(= 4096)$.

other types of scaling, including H as a variable, resulted in much more widely scattered plots. Further, the above result differs from that of Boubnov & Golitsyn (1990) who found f_3 = constant = 0.65.

4.5. *Temperature fluctuation spectra*

Figure 23(a, b) shows typical temperature fluctuation spectra for two rotating convection experiments. As was observed in the non-rotating case, the spectra show a frequency span with a $-\frac{5}{3}$ spectral decay. It is possible to extend the arguments,

based on Eulerian frequency spectra of turbulence, advanced in §3.4, to predict the spectral form. The lengthscale of rotating convective turbulence is limited by $l_r \sim (q_0/\Omega^3)^{\frac{1}{5}}$ and, hence, it is expected that eddies with wavenumbers $k > (q_0/\Omega^3)^{-\frac{1}{5}}$, or frequencies $\omega > \Omega$ exhibit frequency spectra of the form given by (11). It is important, however, to note that the integral velocity scales and lengthscales for the spectra now become $(q_0/\Omega)^{\frac{1}{3}}$ and $(q_0/\Omega^3)^{\frac{1}{5}}$, respectively, and that the scaling for the spectra, analogous to (12), can be written as

$$\frac{E_{T_r}(\omega)}{(\overline{T'^2})_r \Omega^{-1}} \sim \left(\frac{\omega}{\Omega}\right)^{-\frac{5}{3}}. \tag{25}$$

Figure 24(*a*) gives a test for (25) for a series of experiments in which Ω is fixed and q_0 is varied. The collapse of the data in a certain range of high wavenumbers provides support for (25). The range of frequencies compatible with a $-\frac{5}{3}$ decay is somewhat smaller for most experiments than their corresponding non-rotating experiments. This may be due to the low Reynolds number (based on l_r and $(\overline{u'^2})^{\frac{1}{2}}_r$) which results from the inhibition of velocity scales and lengthscales of turbulence by the rotation; further tests are necessary to check this conjecture. Figure 24(*b*) depicts the results of experiments performed at approximately the same q_0 and various Ω. The satisfactory collapse of the data in figure 24(*b*) provides some support for the scaling given in (25). To our knowledge no rotational equivalent of τ has been formulated. It will be of interest to derive such a timescale and to determine normalizing variables for the specta based on it, using an approach similar to that of Boubnov & Ivanov (1988). Boubnov & Golitsyn (1990) have, however, reported that the spectra, in the presence of rotation, show a good collapse when they are scaled with $\overline{T'^2}\tau$ and when ω is scaled with τ, as in the non-rotating case. Nevertheless the non-dimensional spectral values under this scaling are different from those of the non-rotating case.

5. Summary

In the foregoing sections, the results of an experimental study aimed towards improving our understanding of the effects of rotation on convective turbulence were presented. Two sets of experiments, namely convective turbulence in non-rotating and rotating fluids, were performed. The former preceded the latter and acted as a guide to understand the effects of rotation. The experiments were performed in a convection chamber, capable of providing a constant heat flux from below. The ranges of Rayleigh flux number Ra_f and Taylor number Ta investigated were $10^{12} < Ra_f < 10^{13}$ and $10^9 < Ta < 10^{11}$.

The principal results of the non-rotating experiments are as follows:

(i) The vertical and horizontal velocities, and the lengthscale of turbulence, away from the boundaries, scale well with the convective velocity w_* and the height of the convecting layer H, respectively. These velocities are approximately constant in the height interval $0.2 < z/H < 0.8$. The data, in particular those for the horizontal component, compare well with previous results obtained in laboratory tanks and in the atmosphere.

(ii) The r.m.s. buoyancy fluctuations and the mean buoyancy in the core of the convecting layer scale with q_0/w_*.

(iii) Frequency spectra collapse equally well when scaled with either $\overline{T'^2}\tau$ or $\overline{T'^2}(H^2/q_0)^{\frac{1}{3}}$, with the frequency being scaled with τ or $(H^2/q_0)^{\frac{1}{3}}$, respectively. Note that τ is the timescale where thermals are injected into the convective zone from the

conductive boundary layer near the heated surface and $(H^2/q_0)^{\frac{1}{2}}$ is the timescale of the energy-containing eddies of the mixed layer. The scales based on τ were first proposed by Foster (1971) and have been used for scaling temperature fluctuation spectra by Boubnov & Ivanov (1988), whereas the scales based on $(H^2/q_0)^{\frac{1}{2}}$ were introduced in the present study.

The principal results of the rotating experiments are:

(i) The r.m.s. velocities in the mixed layer are affected by the rotation at a height $z \approx 4.5(q_0/\Omega^3)^{\frac{1}{2}}$, or a location where the integral lengthscale is $l_r \approx 1.1(q_0/\Omega^3)^{\frac{1}{2}} \approx 1.5(\epsilon/\Omega^3)^{\frac{1}{2}}$; because of the inhibition of the growth of the lengthscales by the rotation, l_r can also be considered as the lengthscale of the mixed-layer turbulence. The r.m.s. horizontal and vertical velocities within a rotationally affected, convective, mixed layer scale with $(q_0/\Omega)^{\frac{1}{2}}$, with $(\overline{u'^2})^{\frac{1}{2}} \approx 1.6(q_0/\Omega)^{\frac{1}{2}}$ and $(\overline{w'^2})^{\frac{1}{2}}_r/(\overline{u'^2})^{\frac{1}{2}}_r \approx 1$. These results suggest that the Rossby number within the mixed layer is a constant $Ro \approx 0.75$, and that the effects of rotation are quickly felt in all directions even though only the horizontal components are directly affected by the rotation.

(ii) The growth rate of a convective mixed layer in a homogeneous fluid is substantially reduced by the rotation. Although the entrainment-rate data show a good collapse when scaled with the Kolmogorov velocity $(q_0\nu)^{\frac{1}{2}}$ or the r.m.s. velocity of turbulence, $(q_0\Omega)^{\frac{1}{2}}$, implicit evidence provided by the layer-growth data in non-rotating experiments indicates that the latter may be the correct scale.

(iii) Mean buoyancy and r.m.s. buoyancy fluctuations in the core of the mixed layer scale with $(q_0\Omega)^{\frac{1}{2}}$. The mean buoyancy gradient within the convective layer is much larger than that of the non-rotating case. The small size of the integral lengthscale, which restricts the eddy overturning to scales smaller than the depth of the fluid column, was attributed to this observation.

(iv) The temperature spectra were found to scale satisfactorily with $\overline{T'^2}\Omega^{-1}$, when the frequency is scaled with Ω. Further tests are necessary to ascertain the applicability of this scaling to high-Reynolds-number turbulent convection.

The authors wish to thank Mr Steve Ownbey for his able technical help, without which this work could not have been completed. Also thanks are due to Drs P. A. Davies, Boris Boubnov, Eugene Gledzer, E. J. Hopfinger and G. Oth for their numerous comments and suggestions and Varuni Perera for digitizing thousands of particle streaks manually. The referees provided invaluable guidance and help which lead to a significant improvement of the paper. The financial support of the National Science Foundation (Grant No's ATM8514781, MSM8657378) and the Office of Naval Research (Contract No's N00014-87-k-0423 and N00014-88-k-0250) is gratefully acknowledged.

REFERENCES

Adrian, F. J., Ferreira, R. T. D. S. & Boberg, T. 1986 Turbulent thermal convection in wide horizontal layers. *Exps. Fluids* **4**, 121–141.

Bardina, J., Ferziger, J. H. & Rogallo, R. S. 1985 Effect of rotation on isotropic turbulence: computation and modelling. *J. Fluid Mech.* **154**, 321–336.

Boubnov, B. M. & Golitsyn, G. S. 1986 Experimental study of convective structures in rotating fluids. *J. Fluid Mech.* **167**, 503–531.

Boubnov, B. M. & Golitsyn, G. S. 1988 Thermal structure and heat transfer of convection in a rotating fluid layer. *Dolk. Acad. Nauk SSSR* **300**, 350–353.

Boubnov, B. M. & Golitsyn, G. S. 1990 Temperature and velocity field regimes of convective motions in a rotating plane fluid layer. *J. Fluid Mech.* **219**, 215–239.

BOUBNOV, B. M. & IVANOV, V. N. 1988 Time dependent spectrum of temperature fluctuations for free turbulent convection in a fluid layer. *Izv. Atmos. Ocean. Phys.* **24**, 361–367.

BUSSE, F. H. & HEIKES, K. E. 1980 Convection in a rotating layer; a simple case of turbulence. *Science* **208**, 173–174.

CASTAING, B., GUNARATNE, G., HEOLOT, G., KADANOFF, L., LIBCHABER, A., THOMAE, S., WU, X.-Z., ZALESKI, S. & AZNETTI, G. 1989 Scaling of hard thermal turbulence in Rayleigh–Bénard convection. *J. Fluid Mech.* **204**, 1–30.

CAUGHEY, S. J. 1982 Observed characteristics of the atmospheric boundary layer. In *Atmospheric Turbulence and Air Pollution Modelling* (ed. F. T. M. Nieuwstadt & H. VanDop) pp. 107–158. D. Reidel.

CHANDRASEKHAR, S. 1961 *Hydrodynamic and Hydromagnetic Stability*. Dover.

CHEN, R., FERNANDO, H. J. S. & BOYER, D. L. 1989 Formation of isolated vortices in a rotating convecting fluid. *J. Geophys. Res.* **94**, 18445–18453.

CHEN, C. F. & JOHNSON, D. H. 1984 Double diffusive convection: a report on an engineering foundation conference. *J. Fluid Mech.* **138**, 405–416.

COLIN DE VERDIERE. A. 1980 Quasi-geostropic turbulence in a rotating turbulent fluid. *Geophys. Astrophys. Fluid Dyn.* **15**, 213–251.

DANG, K. & ROY, P. 1985 Direct and large-eddy simulation of homogeneous turbulence submitted to solid body rotation. *Proc 5th Symp on Turbulent Shear Flows, Ithaca, NY.*

DEARDORFF, J. W. 1970*a* Preliminary results from numerical investigations of the unstable boundary layer. *J. Atmos. Sci.* **27**, 1209–1211.

DEARDORFF, J. W. 1970*b* Convective velocity and temperature scales for the unstable planetary boundary layer and for Rayleigh convection. *J. Atmos. Sci.* **27**, 1211–1213.

DEARDORFF, J. W. 1972 Numerical investigation of the neutral and unstable planetary boundary layer. *J. Atmos. Sci.* **29**, 91–115.

DEARDORFF, J. W. 1985 Mixed-layer entrainment. A review. In *7th Symp. on turbulence and Diffusion*, (ed. J. C. Weil), pp. 39–42.

DEARDORFF, J. W. & WILLIS, G. E. 1985 Further results from a laboratory model of the convective planetary boundary layer. *Boundary-Layer Met.* **32**, 205–236.

DETERING, H. W. & ETLING, D. 1985 Application of k–ϵ model to the atmospheric boundary layer. *Boundary-Layer met.* **33**, 113–133.

DICKINSON, S. C. & LONG, R. R. 1983 Oscillating grid turbulence including the effects of rotation. *J. Fluid Mech.* **126**, 315–333.

DIKAREV, S. N. 1983 On the influence of rotation on the convective structure in a deep homogeneous fluid. *Dokl. Acad. Nauk. SSSR* **273**, 718–720.

FERNANDO, H. J. S. 1987*a* The formation of layered structure when a stable salinity gradient is heated from below. *J. Fluid Mech.* **182**, 525–541.

FERNANDO, H. J. S. 1987*b* Comments on 'Wind Direction and Equilibrium Mixed-Layer Depth: General Theory'. *J. Phys. Oceanogr.* **17**, 169–170.

FERNANDO, H. J. S., BOYER, D. L. & CHEN, R. 1989 Turbulent thermal convection in rotating stratified fluids. *Dyn. Atmos. Oceans* **13**, 95–121.

FLUERY, M., MORY, M., HOPFINGER, E. J. & AUCHERE, D. 1991 Effects of rotation on turbulent mixing across density interface. *J. Fluid Mech.* **223**, 165–191.

FOSTER, T. D. 1971 Intermittent convection. *J. Geophys. Fluid Dyn.* **2**, 201–217.

FOSTER, T. D. & WALLER, S. 1985 Experiments on convection at very high Rayleigh numbers. *Phys. Fluids* **28**, 455–461.

GOLITSYN, G. S. 1980 Geostrophic convection. *Dok. Acad. Nauk SSSR* **251**, 1356–1360.

GOLITSYN, G. S. 1981 Structure of convection in rapid rotation. *Dok. Acad. Nauk SSSR* **261**, 317–320.

HOPFINGER, E. J. 1987 Turbulence in stratified fluids: A review. *J. Geophys. Res.* **92**, 5287–5303.

HOPFINGER, E. J. 1989 Turbulence and vortices in rotating fluids. *Theor. and Appl. Mech.* (ed. P. Germain, M. Piau & D. Caillerie). Elsevier.

HOPFINGER, E. J., BROWAND, F. K. & GAGNE, Y. 1982 Turbulence and waves in a rotating tank. *J. Fluid Mech.* **125**, 505–534.

HOPFINGER, E. J., GRIFFITHS, R. W. & MORY, M. 1983 The structure of turbulence in homogeneous and stratified rotating fluids. *J. Méc. Theor. Appl.* **44**, 21–82.

HOPFINGER, E. J. & TOLY, J. A. 1976 Spatially decaying turbulence and its relation to mixing across density interfaces. *J. Fluid Mech.* **78**, 155–175.

HOWARD, L. N. 1963 Heat transport by turbulent convection. *J. Fluid Mech.* **17**, 405–432.

HOWARD, L. N. 1966 Convection at high Rayleigh number. In *Applied Mechanics, Proc. 11th Congr. of Appl. Mech., Munich* (ed. H. Görtler), pp. 1109–1115. Springer.

HUNT, J. C. R. 1984 Turbulence structure in thermal convection and shear-free boundary layers. *J. Fluid Mech.* **138**, 161–184.

HUPPERT, H. & TURNER, J. S. 1981 Double diffusive convection. *J. Fluid Mech.* **106**, 299–329.

IBBETSON, A. & TRITTON, D. J. 1975 Experiments on turbulence in a rotating fluid. *J. Fluid Mech.* **68**, 639–672.

JACQUIN, L., LEUCHTER, O., CAMDON, C. & MATHIEU, J. 1990 Homogeneous turbulence in the presence of rotation. *J. Fluid Mech.* **220**, 1–52.

JACQUIN, L., LEUCHTER, O. & GEOFFROY, P. 1989 Experimental study of homogeneous turbulence in the presence of rotation. In *Turbulent Shear Flows* 6 (ed. J.-C. Andre, J. Coustieux, F. Durst, B. E. Launder, F. W. Schmidt & J. H. Whitelaw), pp. 46–57. Springer.

KAIMAL, J. C., WYNGAARD, J. C., HAUGEN, D. A., COTE, O. R., IZUMI, Y., CAUGHEY, S. J. & READINGS, C. J. 1976 Turbulence structure in the convective boundary layer. *J. Atmos. Sci.* **33**, 39–46.

LILLY, D. K. 1968 Models of cloud-topped mixed layers under a strong inversion. *Q. J. Roy. Met. Soc.* **94**, 292–309.

LUNDGREN, T. S. 1985 The vertical flow above the drain-hole in a rotating vessel. *J. Fluid Mech.* **155**, 381–412.

MAXWORTHY, T., HOPFINGER, E. J. & REDEKOPP, L. G. 1985 Wave motions in vortex cores. *J. Fluid Mech.* **151**, 141–165.

MCEWAN, A. D. 1976 Angular momentum diffusion and the imitation of cyclones. *Nature* **260**, 126–128.

MONIN, A. S. 1970 The atmospheric boundary layer. *Ann. Rev. Fluid Mech.* **2**, 225–250.

MORY, M. & CAPERAN, P. 1987 On the genesis of quasi-steady vortices in a rotating turbulent flow. *J. Fluid Mech.* **185**, 121–136.

MORY, M. & HOPFINGER, E. J. 1988 Rotating turbulence evolving freely from an initial quasi 2-D state. In *Macroscopic Modelling of Turbulent Flows* (ed. U. Frish, J. B. Keller, G. Papanicolou & O. Pirenneau). Springer.

NAKAGAWA, Y. & FRENZEN, P. 1955 A theoretical and experimental study of cellular convection in rotating fluid. *Tellus* **7**, 1–21.

ROSSBY, H. T. 1969 A study of Bénard convection with and without rotation. *J. Fluid Mech.* **36**, 309–335.

SALMON, R. 1982 Geostropic turbulence. In *Topics in Ocean Physics*, (ed. R. Mallanotte-Rizzol & A. R. Osborne), North-Holland.

STUBLEY, G. D. & RIOPELLE, G. 1988 The influence of earths rotation on planetary boundary-layer turbulence. *Boundary-Layer Met.* **45**, 307–324.

TENNEKES, H. 1970 Free convection in the turbulent Ekman layer of the atmosphere. *J. Atmos. Sci.* **27**, 1027–1034.

TENNEKES, H. 1975 Eulerian and Lagrangian time microscales in isotropic turbulence. *J. Fluid Mech.* **67**, 561–567.

THOMAS, D. B. & TOWNSEND, A. A. 1957 Turbulent convection over a heated horizontal surface. *J. Fluid Mech.* **2**, 473–492.

TOWNSEND, A. A. 1959 Temperature fluctuations over a heated horizontal surface. *J. Fluid Mech.* **5**, 209–241.

TRAUGOTT, S. C. 1958 Influence of solid body rotation on screen-produced turbulence. *NACA TN* 4135.

TURNER, J. S. 1985 Multicomponent convection. *Ann. Rev. Fluid Mech.* **17**, 11.

TURNER, J. S. 1986 Turbulent entrainment: the development of the entrainment assumption, and its application to geophysical flows. *J. Fluid Mech.* **173**, 431–471.

WIGELAND, R. A. & NAGIB, H. M. 1978 Effect of rotation on decay of turbulence. *Bull. Am. Phys. Soc.* **23**, 998, (also: *IIT Fluids and Heat Transfer Rep.* R78-1).

WILLIS, G. E. & DEARDORFF, J. W. 1984 A laboratory model of the unstable planetary boundary layer. *J. Atmos. Sci.* **31**, 1297–1307.

ZEMAN, O. & LUMLEY, J. L. 1976 Modeling buoyancy driven mixed layers. *J. Atmos. Sci.* **33**, 1974–1988.

ZIMIN, V. D. & KETOV, A. I. 1978 Turbulent convection in a cubic cavity heated from below. *Izv. Acad. Nauk SSSR* **4**, 113–138.